INFORMATION TO USERS

This manuscript has been reproduced from the microfilm master. UMI films the text directly from the original or copy submitted. Thus, some thesis and dissertation copies are in typewriter face, while others may be from any type of computer printer.

The quality of this reproduction is dependent upon the quality of the copy submitted. Broken or indistinct print, colored or poor quality illustrations and photographs, print bleedthrough, substandard margins, and improper alignment can adversely affect reproduction.

In the unlikely event that the author did not send UMI a complete manuscript and there are missing pages, these will be noted. Also, if unauthorized copyright material had to be removed, a note will indicate the deletion.

Oversize materials (e.g., maps, drawings, charts) are reproduced by sectioning the original, beginning at the upper left-hand corner and continuing from left to right in equal sections with small overlaps. Each original is also photographed in one exposure and is included in reduced form at the back of the book.

Photographs included in the original manuscript have been reproduced xerographically in this copy. Higher quality 6" x 9" black and white photographic prints are available for any photographs or illustrations appearing in this copy for an additional charge. Contact UMI directly to order.

UMI

A Bell & Howell Information Company
300 North Zeeb Road, Ann Arbor MI 48106-1346 USA
313/761-4700 800/521-0600

ELECTRON–PHOTON INTERACTIONS IN QUANTUM DOTS: COUPLED OSCILLATORS

BY

SHAUN HOWRIGAN ©

A Dissertation submitted to the Graduate School
in partial fulfillment of the requirements
for the Degree

Master of Science

Major Subject: Physics

Lakehead University
Thunder Bay, Ontario
Canada

November 1995

" Electron–Photon Interactions in Quantum Dots: Coupled Oscillators ," a dissertation prepared by Shaun Howrigan in partial fulfillment of the requirements for the degree, Master of Science , has been approved and accepted by the following:

Dr. M. H. Hawton

Thesis Advisor

Date

ACKNOWLEDGMENTS

This thesis is dedicated to my parents, Clint and Joan, who managed to pass on to me a wonder of the world.

I wish to thank Dr. Margaret Hawton, whose generosity and grace I will remember always. Her patient guidance has made this thesis possible.

The faculty, staff and students of the Physics dept. here at Lakehead have been for me a source of blessed sensiblity and also of many enjoyable, rewarding conversations.

Heartfelt thanks also to my friends and family for their support and patience, especially Randy and Ruth, who have had to deal with the worst of it.

ABSTRACT

ELECTRON–PHOTON INTERACTIONS IN QUANTUM DOTS: COUPLED OSCILLATORS

BY

SHAUN HOWRIGAN

Master of Science

Lakehead University

Thunder Bay, Ontario

Canada, 1993

A coupled oscillator model is developed for the far infra-red response of a quantum dot, and this model is used to predict the vacuum-field Rabi splittings of a dot-cavity system.

Contents

Chapter 1

Heterostructures and Quantum Dots

Introduction

In this thesis it is our aim to demonstrate the effectiveness of employing a coupled harmonic oscillator model (pioneered by Ullersma[2] and refined by Ford, Lewis and O'Connell[3]) to describe the interaction of a quantum dot structure with the electromagnetic field. The quantum dot-EM field serves as an example of a system which can be conveniently modelled as a family of coupled harmonic oscillators, and although chosen only as an example, this system is an attractive choice for several reasons.

Most importantly, recent experiments performed with quantum dots have shown that when subjected to a far infrared probe beam, the electrons in the dot behave as if they were confined in a harmonic potential, making them an ideal candidate for the coupled oscillator model. Also attractive is the analogy that can be made between quantum dots and atoms, since dots, like atoms, posses a discrete level structure (also the product of a central potential) and may be oc-

cupied by one or many electrons. This close correspondence has resulted in the name "artificial atoms" being used in conjunction with quantum dots.

The analogy can be extended to the electrodynamical effects commonly associated with atoms, such as the Lamb shift or stimulated and spontaneous emission. The quantum dot is especially attractive in this case, since the dot-field system can be solved exactly, obviating the need for the pertubation theory approach used in the case of real atoms.

The Evolution of Quantum Dots

Physicists have long realized that spatial confinement of a quantum particle results in the appearance of energetically discrete bound states for the system, an effect encountered in the familiar infinite and finite square well problems. Devices that exhibit this effect were until recently the realm of speculation, but the large body of knowledge and experience developed for the semiconductor electronics industry over the past four decades has made the fabrication of such devices not only possible, but commonplace. The earliest example of engineered quantum confinement in a solid state system is the two-dimensional electron gas (2DEG) in a silicon inversion layer, produced in 1966 by Fowler[5] et al., which sparked research into two-dimensional systems that continues to this day.

Our increasing ability to control matter at fine scales is what drives the fabrication of devices that show higher degrees of spatial confinement, and so ad-

vancements in fabrication technologies or techniques lead almost immediately to new or improved devices. Perhaps the single most important advance that has had an impact on modern device technology is the epitaxial growth of ultra-thin films, which allowed the first semiconductor quantum well to be built at Bell Labs by Dingle[6] et. al. in 1974. The performance of these early quantum wells were limited by their low carrier mobilities, however, and it was this limitation that lead to another major advance, modulation doping.

The technique of modulation doping, where the impurity atoms that supply carriers are spatially separated from the carriers themselves, results in conduction with greatly reduced impurity scattering and hence very high electron mobilities. The energy band diagrams below illustrate the modulation doping technique.

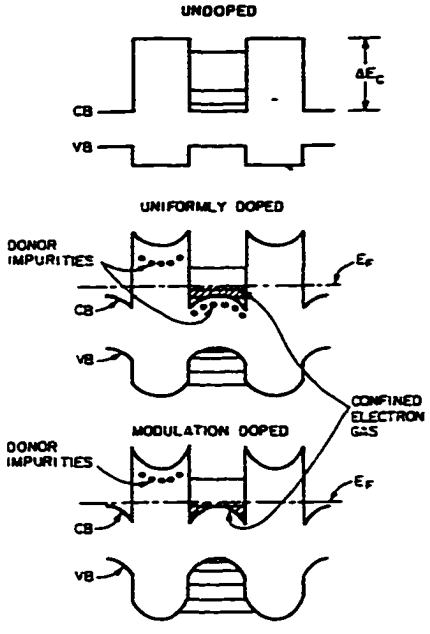

FIG. 1. Energy-band diagrams for n-doped and undoped GaAs-$Al_xGa_{1-x}As$ superlattices.

In 1990, GaAs/AlGaAs heterojunctions had electron mobilities in the range of 10^7 $\frac{cm^2}{V-s}$, resulting in exceptionally high quality 2DEG's in quantum wells. These high mobility quantum wells have in turn made the investigation of ballistic electron transport in semiconductors an experimental reality, and this has become another active field of both theoretical and experimental research.

Higher mobility implies both a longer mean free path length and coherence length, and it was in anticipating the implications of these extended path lengths in quantum wells in 1969 that Esaki and Tsu proposed the idea of an engineered superlattice structure, what Esaki[7] calls "do-it-yourself quantum mechanics". Their basic idea was that the conduction and valence band edges could be spa-

tially varied in a semiconductor structure by either modulating the doping or composition of the device. So long as the coherence length exceeds the spatial period of the modulation, the carriers can sample these variations, and the superlattice device will display a dispersion which is potentially much different than that of the semiconductor material. Progress in this field has resulted in the ability to design and build devices with customized band diagrams, at least for the case of electron propagation perpendicular to the plane of the well (i.e., in the growth direction).

Parallel to the plane of the well, however, the carriers will remain free unless a lateral potential is imposed on the 2DEG. And while the epitaxial techniques have matured to give us considerable control of potentials in the growth directions of these heterostructure devices, the ideas and methods required for the same degree of control of lateral potentials in these devices are in their infancy. In fact, it was not until the mid 1980's that fabricated nanostructures (i.e., devices that exhibit quantum confinement in more than one spatial dimension) were first constructed, due primarily to advances in electron and optical lithographic techniques. At present, the minimum lateral dimension attainable with either of these techniques is about 15 nm, which results in confinement energies of up to 30 meV. The hope is that with an improved technology of lateral confinement, heterojunction devices could have energy level spacings in the hundreds of meV's range (Reed[8], p6). This would lead to hosts of new engineered devices, both electronic and

optoelectronic, that would display fully quantized behavior. The implications of such a technology are difficult to accurately speculate on, but it will most certainly heavily impact the information industry, and most probably many others.

Although devices that employ lateral confinement potentials are not currently manufactured commercially, they are the subject of intense industrial and academic research. Quantum wires, structures with carriers confined in the growth and one lateral dimension, and quantum boxes, structures with carriers confined in the growth and both lateral dimensions, are currently fabricated and characterized in many research labs. (In this thesis we deal with a specific example of a quantum box, the quantum dot, which is characterized by a lateral confining potential which is parabolic in both lateral dimensions). The techniques employed in the fabrication of these devices are at present quite varied and quickly changing as researchers find new and better means of producing lateral confinement in structures. In the case of quantum wires, a slightly more mature field than that of quantum dots, clever growth techniques developed by P.M. Petroff[9] et. al. at AT&T Bell Labs. in 1984 are now used in the production of high quality quantum wire arrays. In those cases where single quantum wires are desirable, Kapon[10] et. al.(1989) of Bellcore have found ways of growing high quality V-groove quantum wires using organometallic chemical vapor deposition.

In the case of quantum dots, however, the fabrication techniques are more primitive, involving physically and\or chemically etching wafers to produce cylin-

drical columns (Reed[13] et. al. 1987), or chemically precipitating spherical clusters (nanocrystallites) of semiconductor material onto surfaces (Oshinowo[14] et. al., 1994) or into polymer matrix materials (Salata[15] et. al., 1994). Both methods originally displayed serious drawbacks, but continued effort has served to resolve some of these difficulties.

The impetus behind this considerable effort is a technological one, stemming from the benefits reduced dimensionality bring to optoelectronic semiconductor devices. Most importantly, the more sharply peaked electron density of states associated with confined systems results in a highly selective gain profile for such systems (narrower linewidths), while the reduced volume of the active medium required for spatial confinement means there are fewer electron-hole pairs available for population inversion, which in turn means that a very small current will be required to reach inversion (typically microamps, Kapon[10] et. al., 1989). These benefits make low-dimensional structures ideal candidates for solid-state lasers, and indeed this is the most active area of research and development associated with these structures. Lasing action requires of course that the low-dimensional devices be placed in a tuned cavity which supports modes that overlap the peaks in the gain profile of the active medium. In practice, this is accomplished by integrating the devices with a pair of distributed Bragg reflectors (DBR), although it may also be possible to place them in a micro-machined confocal cavity. Again, this technology is more developed in the case of quantum wires than for the case

of quantum dots.

In the case of quantum wire arrays in a DBR cavity, the geometry of the vertical cavity surface emitting laser is the natural choice of the designer, and high quality quantum wire array microcavity lasers have been constructed recently based on this geometry (Chavez-Pirson[11] et. al., 1994). The case of quantum dots in a cavity has been more problematic, since physically integrating the dot structures into a DBR cavity necessitates overgrowing the dots with some suitable matrix material, a process which so far has shown limited success. This does not deter theoretical speculation, however, and the subject of a quantum dot in a resonant cavity is an interesting problem in its own right, one with both theoretical and practical aspects. In fact, this problem is closely related to another active field of research, namely cavity quantum electrodynamics (QED), but more specifically to the study of atoms in optical cavities. The analogy is an attractive one, since the discrete level structure of quantum dots has already earned them the nickname "artificial atoms". What we are considering here could then be called "cavity QED with artificial atoms", and as we progress the analogy will reveal itself in the mathematics of the system.

A discussion of the dynamics of the quantum well or quantum dot-DBR cavity system is in actuality a discussion of the interaction between the modes of the spatially confined electron system and the modes of the electromagnetic (EM) field in the cavity. For the case of the quantum well-DBR cavity structure, Weisbuch[12]

et. al. observed in 1992 that exciton polaritons are formed in the well when the structure is resonantly excited. This behavior is similar to another well-studied system, that of an atom in a confocal cavity, where researchers (Rempe[16] et. al., Zhu[17] et. al.) have observed vacuum Rabi splitting in the transmitted spectrum of the atom-cavity system as a probe beam was scanned through resonance. Zhu et. al. state that this behavior can be explained by a completely classical model, which is surprising in light of the fact that the atom is a fully quantum entity and that the intensity of the probe beam is such that the fundamental cavity mode is occupied by zero or one quanta.

As mentioned previously, here we are considering the case of quantum dots, which means the confining potential is parabolic in the lateral dimensions, and so the electron system sees a simple harmonic oscillator potential. Interacting with this electron oscillator is the electromagnetic field, which itself is modeled as a heat bath of independent quantum oscillators, and so we end up with the situation of a harmonic oscillator coupled to a heat bath of quantum oscillators. This is a venerable problem in physics, and one of its most recent and complete treatments has been given by Ford, Lewis, and O'Connell in the context of developing the quantum Langevin equation[4] in 1988. The beauty of this model of an electron interacting with the EM field is that the solution for the system frequencies is exact, as shown by Ullersma in 1966 (the eigenvectors will have to be found numerically, however). This also holds in the quantum case, since in

the Heisenberg picture the equations of motion for the operators take exactly the same form as their classical counterparts.

The situation becomes more complex when we consider more than one electron in the harmonic potential, since the Coulomb interaction between electrons makes this a many body problem. The solution of these systems is more difficult, and when we have more than 4 electrons we rely solely on numerical methods for a complete description of the system dynamics. There is, however, one situation for which we may still obtain an exact solution for some of the system dynamics. This is the case when we treat this problem in the dipole approximation, meaning that the wavelength of the EM field modes is large enough to guarantee constant field intensity over the region occupied by the quantum dot. Kohn[1] showed in 1961 that the centre of mass of such a system of N electrons in a magnetic field behaves like a single particle of mass Nm and charge Ne coupled to the electromagnetic field, and his work on the subject has become known as Kohn's theorem. This means that the system of electrons in a dot appears as a single particle whose charge we can select. This selectable charge affords an excellent opportunity to investigate self-field effects equivalent to the Lamb shift and spontaneous emission in atoms.

Kohn's theorem has since been extended, largely due to work done on semiconductor nanostructures such as parabolic quantum wells, wires and quantum dots, and is now known as the generalized Kohn's theorem (GKT, Brey[18] et. al.) and

the Harmonic Potential Theorem (HPT, Dobson[19], Yip[20]). The experimental record on quantum dots confirms the validity of these theoretical assumptions, and because dots are very young (the first being successfully demonstrated in 1988 by Reed[13] et. al.), it is relatively easy to track the experiments that motivated the theoretical developments, and vice versa.

Ciebert[21] et. al., working at AT&T in New Jersey in 1986, demonstrated carrier confinement to one and zero degrees of freedom in GaAs-GaAlAs structures. Using low temperature cathodoluminescence, they found luminescence lines which they attributed to transitions between ground and excited states in their fabricated devices. Motivated by these and other contemporary experiments also demonstrating low dimensional confinement, in 1987 Bryant[22] calculated the states for a few interacting electrons confined to small (10 to 1 nm) boxes. As expected, the level structure became very complicated for interacting multi-electron systems.

Early experiments which probed dots through their interaction with far infrared light observed a much simpler spectrum than predicted by the many body models of Bryant and others (Laughlin[23], Kirsenow[24], Pfannaguche[25]), and several researchers made the observation that the dots were exhibiting spectra with the same level structure as a single electron in a parabolic potential (Sikorski & Merkt[26], in 1989; Liu[27] et. al., in 1989; Demel[28] et. al., in 1990). Such a single electron system had been treated by V. Fock[29] in 1928, whose results

predicted the same spectra recorded in the FIR quantum dot measurements, a fact which was quoted often in the original experimental literature. Bryant's calculations had made apparent the fact that level structure was highly dependent on many body effects, yet the experimental results seemed to indicate the opposite: that level structure was independent of the number of electrons occupying the dot. This was explained rigorously in 1990 by Maksym and Chakraborty[30] and also Bakshi, Broido and Kempa[31] in terms various versions of the Generalized Kohn's Theorem. The essential observation in each case is that for a harmonic confinement potential, the Hamiltonian of the system separates into relative and centre of mass terms, and in the dipole approximation, light couples only to the centre of mass term. This is the state of quantum dot models today. An exact solution is available for FIR spectra, and numerical solutions are used for those cases where the dipole approximation does not apply or the confining potential is non-parabolic.

Our Approach to the Quantum Dot

In this thesis, an investigation is made of the behavior of quantum dots in perpendicular magnetic fields and probed with light ranging from microwave to near infrared frequencies. Consequently, only the centre of mass solution is presented explicitly, although we begin with a more general description of the system. Following a discussion of the two dimensional electron gas (2DEG), our approach here

is to begin with the classical Lagrangian (in the Coulomb gauge) for an arbitrary distribution of electrons in a harmonic oscillator potential and interacting with a vector potential describing both the magnetic and FIR fields. The Lagrangian is then transformed to reciprocal space since the interaction between the electrons and field modes is most apparent in the k-space representation. Additionally, complex coordinates for electron position and the vector potential are introduced. This is motivated by the fact that electrons in magnetic fields follow circular orbits, which can be concisely described with complex coordinates, and by the fact that photons coupled to such a system will display circular polarization. The resulting reciprocal space Lagrangian is a real function of complex coordinates. Following the early work of Ullersma and the more recent work of Ford, Lewis and O'Connell the Lagrangian can be written as an ensemble of interacting oscillators. Lagrange's equation then yields the equations of motion for the system. These equations for the electrons and the fields display coupling between the particle momenta and the field coordinates, what Ford et. al. call velocity coupling. Additionally, the Coulombic electron-electron interaction remains present in the equation of motion for the electrons. At this stage the problem is still general, and can in principle be solved for both the relative (many-body) motion as done by Laughlin for the case of three electrons in a magnetic field or by Maksym and Chakraborty for quantum dots in a magnetic field, or for the centre of mass (collective) motion, which has been done by many authors in the context of dis-

cussing FIR absorption in quantum wells. The solution in the many body case will by necessity be numerical in nature if more than a few electrons are present. In contrast to this is the centre of mass case, which has been shown to posses an exact solution, regardless of the number of electrons present, making it attractive theoretically. Moreover, since we are investigating the FIR case here, the centre of mass solution will be sufficient to describe the dynamics of our system.

In fact, it is because we are in the FIR limit that an exact solution is possible. In this limit, with the electron in a magnetic field (or any other harmonic potential), Kohn's theorem states that the electron-electron interactions do not affect the absorption spectrum of the electron-magnetic field system, which displays a narrow resonance at the cyclotron frequency. This means that in the centre of mass case, the Coulomb interaction term is not coupled to the field and does not affect the centre of mass equation of motion and so we can solve the system exactly. This gives us the dispersion relation for the system, from which we can graphically determine the system frequencies, as well as investigate the behavior of the system under circumstances such as varying FIR and magnetic field frequencies.

Although a Lagrangian is completely adequate for our purposes here, it is also advantageous to employ a Hamiltonian approach, for the reasons that the translation to quantum mechanics is more straightforward in that formalism. Consequently, we also write the Hamiltonian for the system. This also allows a simple

demonstration of the independence of centre of mass and relative coordinates for the quantum dot in the dipole approximation, and shows that the proposed solutions block diagonalize the Hamiltonian.

Chapter 2

Modelling the Quantum Dot

The Two Dimensional Electron Gas

Much of the behavior of the quantum dot stems from the dynamics of the underlying two-dimensional electron gas (2DEG) upon which the dot's parabolic confinement potential is imposed. A brief review of the properties of 2DEG's which apply to our treatment of dots will be helpful in the understanding of the system. This review contains by necessity only a small portion of the vast body of literature on the subject, that which applies most immediately to this analysis of quantum dots.

2DEG's manifest themselves in several physical structures: in thin films, in insulator-semiconductor interfaces (inversion layers) and semiconductor-semiconductor junctions (heterostructures), or on the surface of liquid helium. The defining characteristic in these situations is that the carriers are free to move in the two spatial dimensions parallel to the film or junction or liquid surface, but are confined in the third spatial dimension, the direction perpendicular to the interface, and consequently have quantized energy levels in that dimension. These systems are not truly two-dimensional, however, as the electron wavefunction will have some

small but finite extent in the perpendicular dimension. Furthermore, the electronic system couples to the electromagnetic field, which is not confined to the plane.

One can, however, as a first approximation, treat the system two-dimensionally in an attempt to determine the energy level structure and dynamical behavior of the 2DEG. It was J.R. Schreiffer[33], studying inversion layers in silicon, who pointed out that if the carrier wavelength was of the same magnitude as the distance from the interface to the classical turning point, the behavior of the carrier in the interface would have to be treated quantum-mechanically, since penetration of the carrier wavefunction into the barrier is a strictly quantum effect. In order to justify the assumption that the electron's behavior is essentially two–dimensional in quantum dots, we consider a well known example from the experimental literature.

Reed[13] et. al. have demonstrated fully quantized energy level structure in an AlGaAs-InGaAs quantum dot structure. Using electronic spectroscopy on a 50 $\AA$ quantum well layer the group observed two transmission peaks, a ground state resonance at 50 mV and an excited state resonance at 700 mV. Subsequent measurements on quantum dots based on the same quantum well geometry show finer structure superposed on these quantum well resonances. This finer structure consists of equally spaced oscillator modes with a level spacing of 50 mV. From this one can see that across a broad range of energies (i.e., 50 to 700 mV), only

the first subband of the quantum dot will be occupied, and so the assumption of two-dimensional behavior is justified.

Generally, treating the interface potential is a complex problem, depending on the type of physical structure being investigated (e.g. a MOS junction like Si-SiO_2 or a heterojunction such as GaAs-$Al_xGa_{1-x}As$ which may have a grading of the junction interface that ranges from abrupt to very gradual). These treatments comprise an extensive literature in themselves, with ongoing debate as to the proper methods and techniques with which to approach the problem. The most common treatment is a self-consistent solution of Schrödinger's and Poisson's equations, evaluated numerically. The work of Stern and Howard[34] is representative of these original self-consistent solutions. More recent work incorporates the use of exchange and correlation potentials, which becomes increasingly important at low carrier densities, a region of particular interest for quantum dots. The most effective approach has been the density-functional method developed by Hohenberg[36] and Kohn, and Kohn[37] and Sham in 1965, which Ando[35] applied to the space-charge layer in silicon in 1976.

An electron constrained in the z dimension by an interface potential will display an energy structure like

$$E = E_z + \frac{\hbar^2}{2m^*}\left(k_x^2 + k_y^2\right),$$

where E_z denotes discrete level structure determined by the interface potential, $k_x$and k_y are the wavevector components parallel to the interface, and m^* is the

effective mass of the carrier moving parallel to the interface. This gives rise to a subband structure with the discrete values of E_z defining the bottom of each subband. As the energy of electrons at the interface rises past the energy levels determined by E_{z1}, E_{z2}, etc., the high energy electrons will begin to fill the higher-order subbands consecutively. As we have already noted, the calculation of the discrete level structure can be complicated for interfaces. A more realistic treatment of the interface models the interface potential as a finite square or triangular well, in which case graphical or numerical solutions are necessary when determining the energy eigenvalues of the system. The deeper the actual finite well, the better an approximation the infinite square well becomes, especially for the lowest-lying levels.

In the case of quantum well heterostructures, however, the modelling of the junction by a finite square-well potential is a reasonably realistic approach, supported by the experimental literature. As a first approximation to the square well, we can assume an idealized heterojunction with infinite barriers, and employ the effective mass approximation to find the familiar energy band structure

$$E_{n,k} = \frac{\hbar^2}{2m_z}\frac{\pi^2}{d^2}n^2 + \frac{\hbar^2 k^2}{2m^*},$$

where m_z is the effective mass for carrier displacement at right angles to the plane of the well, m^* is the effective carrier mass for motion parallel to the well, k ($k^2 = k_x^2 + k_y^2$) is the wavevector for motion parallel to the well, and d is the physical width of the well. With a definite expression for the energy levels of the

2DEG, we are able to determine the density of states (DOS) explicitly.

If we use the infinite square well model of the well with the effective mass approximation, the density of states $\left(D_2(E_{n,k}) = \frac{dN}{dE_{n,k}}\right)$ in two dimensions becomes:

$$D_2\left(E_{n,k}\right) = n\frac{g_v m^*}{\pi\hbar^2}\left(L_x L_y\right). \tag{2.1}$$

where g_v accounts for any degeneracy in the energy band structure of the semiconductor. The curves below demonstrate the effect of dimensional confinement on the density of states of an electron gas.

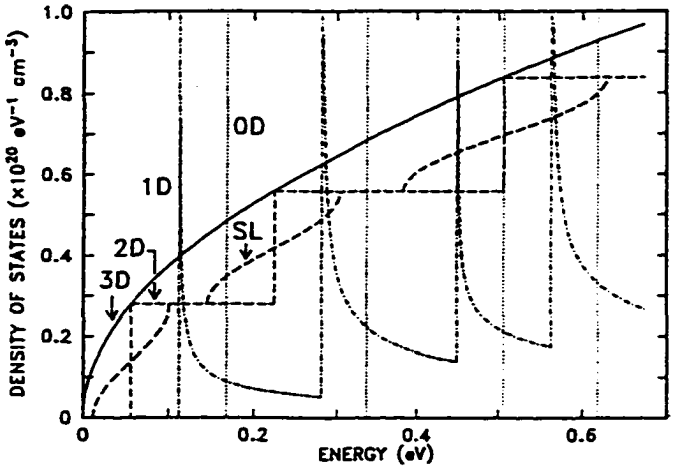

Fig. 1 Comparison of density of states in the three-dimensional (3D) electron system with those of a superlattice, and the two-dimensional (2D), one-dimensional (1D), and zero-dimensional (0D) electron systems

In the case of quantum dots, the quantum well is more accurately modelled with a finite square well potential, which will also yield discrete energy levels, but which does not posses a convenient analytical expression.

While the density of states presented in eq.(2.1) is satisfactory for electrons

which are free to move in two dimensions, it does not describe the DOS for a quantum dot (in or out of a magnetic field). A correct expression for the DOS in a quantum dot must account for the spatial confinement owing to the parabolic confinement potential found in dots also and the perpendicular magnetic field acting on the 2DEG discussed above. Without explicitly calculating the DOS for a quantum dot, we can anticipate some characteristics of its structure. First, the dot density of states will be a collection of delta function peaks spaced according to the energy level structure of the dots, which is a characteristic possessed generally by any zero-dimensional system (see Fig. 1). These peaks will be characterized by three quantum numbers, as in any zero-dimensional quantum system, and will be broadened by various mechanisms (such as emissions into available EM and phonon modes), in much the same way that atomic energy levels are broadened.

Lagrangian Treatment and Equations of Motion

The physical system we deal with here, the quantum dot, can be described as an electron gas strongly confined in the z-direction (i.e. a 2DEG), laterally confined by a harmonic potential, and immersed in a static external magnetic field, **B**. This dot is then probed with a FIR field. Our treatment of the system dynamics considers only the centre of mass motion of the system, and the effect of electron-electromagnetic field interactions.

We begin by writing the classical Lagrangian for the system in the Coulomb

gauge,

$$L = \sum_{\alpha} \frac{m^*}{2} \left(\dot{\mathbf{r}}_\alpha^2 - \omega_0^2 \mathbf{r}_\alpha^2 \right) - V_{coul} + \frac{\varepsilon}{2} \int d^3r \left[\dot{\mathbf{A}}^2 - c^2 \left(\nabla \times \mathbf{A} \right)^2 \right] + \int d^3r \, \mathbf{j} \cdot \mathbf{A},$$

where $\mathbf{r}_\alpha(t)$ is the position vector for the αth particle, $\mathbf{A}(\mathbf{r}, t)$ is the vector potential, and $\mathbf{j}(\mathbf{r}, t)$ is the current density.

In this case we deal with point charges, namely electrons, so

$$\mathbf{j}(\mathbf{r}, t) = -\sum_{\alpha} e \dot{\mathbf{r}}_\alpha \delta \left(\mathbf{r} - \mathbf{r}_\alpha \right).$$

Furthermore, we can break the vector potential into a dynamic (time-dependent) part, $\mathbf{A}_D$, and a static (time-independent) part, $\mathbf{A}_S$, so that $\mathbf{A}(\mathbf{r}, \mathbf{t}) = \mathbf{A}_S(\mathbf{r}) + \mathbf{A}_D(\mathbf{t})$. This works well in our case since the magnetic field turns out to be completely independent of time, whereas the FIR probe is a harmonic function of time. This division of the vector potential yields

$$\begin{aligned} L \;=\; & \sum_{\alpha} \frac{m^*}{2} \left(\dot{\mathbf{r}}_\alpha^2 - \omega_0^2 \mathbf{r}_\alpha^2 \right) - V_{coul} + \frac{\varepsilon}{2} \int d^3r \left[\dot{\mathbf{A}}_D^2 - c^2 \left(\nabla \times \mathbf{A}_D \right)^2 \right] - e \sum_{\alpha} \dot{\mathbf{r}}_\alpha \cdot \mathbf{A}_D \\ & - e \sum_{\alpha} \dot{\mathbf{r}}_\alpha \cdot \mathbf{A}_S. \end{aligned}$$

At this point it is advantageous to work with our dynamic field terms in k-space, since these are the normal modes for the electromagnetic field, and this leads to a simpler representation for the Lagrangian. Defining the Fourier transform pair as

$$\mathbf{A}_D(\mathbf{r}, t) \;=\; \frac{1}{(2\pi)^{\frac{3}{2}}} \int d^3k A(\mathbf{k}, t) \exp(i\mathbf{k} \cdot \mathbf{r}),$$

$$A(\mathbf{k},t) = \frac{1}{(2\pi)^{\frac{3}{2}}}\int d^3r \mathbf{A}_D(\mathbf{r},t)\exp(-i\mathbf{k}\cdot\mathbf{r}),$$

and employing the Parseval-Plancherel identity

$$\int d^3r\, F^*(\mathbf{r})\, G(\mathbf{r}) = \int d^3k\, \mathcal{F}^*(\mathbf{k})\, \mathcal{G}(\mathbf{k}),$$

we find

$$\begin{aligned} L &= \sum_\alpha \frac{m^*}{2}\left(\dot{\mathbf{r}}_\alpha^2 - \omega_0^2\mathbf{r}_\alpha^2\right) - V_{coul} + \frac{\varepsilon}{2}\int d^3k\left[\dot{A}(\mathbf{k},t)^2 - c^2(i\mathbf{k}\times A(\mathbf{k},t))^2\right] \\ &\quad -e\frac{1}{(2\pi)^{\frac{3}{2}}}\sum_\alpha \dot{\mathbf{r}}_\alpha\cdot\int d^3k\dot{A}(\mathbf{k},t)\exp(i\mathbf{k}\cdot\mathbf{r}) - e\sum_\alpha \dot{\mathbf{r}}_\alpha\cdot\mathbf{A}_S. \end{aligned}$$

We can discretize the integrals using periodic boundary conditions, which results in the prescription

$$\int d^3k \rightarrow \frac{(2\pi)^3}{V}\sum_k,$$

giving us

$$\begin{aligned} L &= \sum_\alpha \frac{m^*}{2}\left(\dot{\mathbf{r}}_\alpha^2 - \omega_0^2\mathbf{r}_\alpha^2\right) - V_{coul} + \frac{\varepsilon}{2}\frac{(2\pi)^3}{V}\sum_{k,\lambda}\left[\dot{A}_{k,\lambda}^2 - c^2\left|i\mathbf{k}\times A_{k,\lambda}\right|^2\right] \\ &\quad -e\frac{(2\pi)^{\frac{3}{2}}}{V}\sum_{\alpha,k,\lambda}\dot{\mathbf{r}}_\alpha\cdot\dot{A}_{k,\lambda}\exp(i\mathbf{k}\cdot\mathbf{r}_\alpha) - e\sum_\alpha \dot{\mathbf{r}}_\alpha\cdot\mathbf{A}_S. \end{aligned}$$

Where the summation is over k, the field modes, and λ, the field polarizations. Noting that $(i\mathbf{k}\times A)^*\cdot(i\mathbf{k}\times A) = k^2A^2$, and defining an oscillator coordinate $\mathbf{q}_k = \frac{e(2\pi)^{\frac{3}{2}}}{m_k\omega_k V}\exp(i\mathbf{k}\cdot\mathbf{r}_\alpha)A_k$ for each EM field mode, we find

$$L = \sum_{\alpha} \frac{m^*}{2}\left(\dot{\mathbf{r}}_\alpha^2 - \omega_0^2 \mathbf{r}_\alpha^2\right) - V_{coul} + \frac{\varepsilon V}{2e^2}\sum_j m_j^2\omega_j^2\left[\dot{\mathbf{q}}_j^2 - \omega_j^2\mathbf{q}_j^2\right] - \sum_{\alpha j} m_j\omega_j\dot{\mathbf{r}}_\alpha\cdot\mathbf{q}_j$$
$$- e\sum_{\alpha}\dot{\mathbf{r}}_\alpha\cdot\mathbf{A}_S,$$

where the summation over field modes and polarizations has been simplified to $\sum_j = \sum_{k\lambda}$.

In the same manner as Ford, Lewis and O'Connell we define a new quantity, m_j, as

$$m_j = \frac{e^2}{\varepsilon V\omega_j^2}, \tag{2.2}$$

which has the dimensions of mass, and which allows us to write the field energy term in the Lagrangian as a harmonic oscillator term, so our Lagrangian becomes

$$L = \sum_{\alpha}\frac{m^*}{2}\left(\dot{\mathbf{r}}_\alpha^2 - \omega_0^2\mathbf{r}_\alpha^2\right) + \sum_j \frac{m_j}{2}\left[\dot{\mathbf{q}}_j^2 - \omega_j^2\mathbf{q}_j^2\right] - V_{coul} - \sum_{\alpha j} m_j\omega_j\dot{\mathbf{r}}_\alpha\cdot\mathbf{q}_j - e\sum_\alpha \dot{\mathbf{r}}_\alpha\cdot\mathbf{A}_S.$$

Note that the Lagrangian now looks like a family of two-dimensional electron oscillators (experiencing the Coulomb interaction) coupled through the $\mathbf{j}\cdot\mathbf{A}$ term to a family of two-dimensional field oscillators.

Two definitions will allow us to write our Lagrangian as a real function of complex coordinates, taking advantage of the system's inherent rotational symmetry. The first definition, $z_\alpha = x_\alpha + iy_\alpha$, is the normal mode coordinate for the electron-magnetic field system[1]. The second definition, $q = q_x + iq_y$, anticipates the circularly polarized normal modes of the EM field coupled to this electron-magnetic field system. The time derivatives of these complex coordinates can be

written as $\dot{z}_\alpha = \dot{x}_\alpha + i\dot{y}_\alpha$, and $\dot{q} = \dot{q}_x + i\dot{q}_y$. In terms of these new coordinates, our Lagrangian is (see Appendix A for details)

$$\begin{aligned} L &= \sum_\alpha \frac{m^*}{2}\left(\dot{z}_\alpha \dot{z}_\alpha^* - \omega_0^2 z_\alpha z_\alpha^*\right) + \sum_j \frac{m_j}{2}\left(\dot{q}_j \dot{q}_j^* - \omega_j^2 q_j q_j^*\right) \\ &\quad - \sum_{\alpha j} \frac{m_j \omega_j}{2}\left(\dot{z}_\alpha q_j^* + \dot{z}_\alpha^* q_j\right) - e\sum_\alpha \dot{\mathbf{r}}_\alpha \cdot \mathbf{A}_S \\ &\quad - V_{coul}\left(|z_\alpha - z_\beta|\right). \end{aligned}$$

At this point we abandon generality in the static vector field, $\mathbf{A}_s$, and specify a magnetic field $\mathbf{B}_0$, perpendicular to the plane of the 2DEG. Hence $\mathbf{A}_s = \frac{B_0}{2}(-y, x, 0)$, and

$$\begin{aligned} L &= \sum_\alpha \frac{m^*}{2}\left(\dot{z}_\alpha \dot{z}_\alpha^* - \omega_0^2 z_\alpha z_\alpha^*\right) + \sum_j \frac{m_j}{2}\left(\dot{q}_j \dot{q}_j^* - \omega_j^2 q_j q_j^*\right) \\ &\quad - \sum_{\alpha j} \frac{m_j \omega_j}{2}\left(\dot{z}_\alpha q_j^* + \dot{z}_\alpha^* q_j\right) - \frac{eB_0 i}{4}\sum_\alpha \left(z_\alpha \dot{z}_\alpha^* - z_\alpha^* \dot{z}_\alpha\right) \\ &\quad - V_{coul}\left(|z_\alpha - z_\beta|\right). \end{aligned} \tag{2.3}$$

This, then, is our classical Lagrangian. Our equations of motion are derived from the Lagrange equations, $\frac{d}{dt}\left(\frac{\partial \mathcal{L}}{\partial \dot{z}_\alpha^*}\right) - \frac{\partial \mathcal{L}}{\partial z_\alpha^*} = 0$ and $\frac{d}{dt}\left(\frac{\partial \mathcal{L}}{\partial \dot{q}_j^*}\right) - \frac{\partial \mathcal{L}}{\partial q_j^*} = 0$, and likewise for z_α, and q_j. We first consider the variables z_α^* and q_j^*, with their resulting equations of motion being

$$\left(\frac{m^*}{2}\ddot{z}_\alpha - \frac{eB_0 i}{2}\dot{z}_\alpha + \frac{m^*}{2}\omega_0^2 z_\alpha\right) - \sum_j \frac{m_j \omega_j}{2}\dot{q}_j + \frac{\partial V_{coul}}{\partial z_\alpha^*} = 0, \tag{2.4}$$

and

$$\ddot{q}_j + \omega_j^2 q_j + \omega_j \sum_\alpha \dot{z}_\alpha = 0. \tag{2.5}$$

Note that these equations of motion govern the behavior z_α and q_j, respectively. We could also write the equations of motion for z_α^* and q_j^*, but this proves to be unnecessary since they would simply be the complex conjugates of the equations of motion shown above. This redundancy in the equations of motion results from the use of complex coordinates and their corresponding effect on the apparent degrees of freedom of the system. This is discussed further in appendix A.

If we work in the dipole limit, i.e., assume the external electric field is constant over the dimension of the dot, we can apply the generalized Kohn's theorem and so the electron-electron interactions do not couple to the centre of mass coordinate, eliminating the $\frac{\partial V_{coul}}{\partial z_\alpha^*}$ term. It is possible to express the equations of motion in terms of the centre of mass coordinates of the electrons in the dot. If we define the electron centre of mass coordinate as

$$Z_{cm} = \frac{1}{N} \sum_\alpha^N z_\alpha ,$$

and sum the equation of motion for the electrons (eq.2.4) over the electron index, α, we find

$$\sum_\alpha \left\{ \left(m^* \ddot{z}_\alpha - eB_0 i \dot{z}_\alpha + m^* \omega_0^2 z_\alpha \right) - \sum_j m_j \omega_j \dot{q}_j = 0 \right\},$$

or, equivalently

$$m^* \sum_\alpha \ddot{z}_\alpha - eB_0 i \sum_\alpha \dot{z}_\alpha + m^* \omega_0^2 \sum_\alpha z_\alpha - N \sum_j m_j \omega_j \dot{q}_j = 0.$$

Note that the common factor of $\frac{1}{2}$ has been eliminated from the equation of motion for z_α. In terms of the electron centre of mass coordinates, Z_{cm}, this becomes

$$m^* \ddot{Z}_{cm} - eB_0 i \dot{Z}_{cm} + m^* \omega_0^2 Z_{cm} = \sum_j m_j \omega_j \dot{q}_j, \tag{2.6}$$

and the equation of motion for the jth field coordinate (eq.2.5) becomes

$$\ddot{q}_j + \omega_j^2 q_j = -N \omega_j \dot{Z}_{cm}. \tag{2.7}$$

Note that we have a quadratic Lagrangian, which suggests solutions of the form: $Z_{cm}(t) = Z_0(\omega) e^{-i\omega t}$ and $q_j(t) = q_{j0}(\omega) e^{-i\omega t}$. Substitution into our equations of motion yields

$$\left(-m^* \omega^2 - eB_0 \omega + m^* \omega_0^2\right) Z_0(\omega) = -i\omega \sum_j^n m_j \omega_j q_{j0}(\omega) \tag{2.8}$$

$$\left(-\omega^2 + \omega_j^2\right) q_{j0}(\omega) = iN\omega\omega_j Z_0(\omega). \tag{2.9}$$

This system of equations in Z_0 and q_{j0} supports a solution if the determinant

of the coefficient matrix vanishes, i.e.,

$$\begin{vmatrix} (-m^*\omega^2 - eB_0\omega + m^*\omega_0^2) & -i\omega m_1\omega_1 & -i\omega m_2\omega_2 & \cdots & -i\omega m_n\omega_n \\ -iN\omega m_1\omega_1 & m_1\left(-\omega^2+\omega_1^2\right) & 0 & \cdots & 0 \\ -iN\omega m_2\omega_2 & 0 & m_2\left(-\omega^2+\omega_2^2\right) & \cdots & 0 \\ \vdots & \vdots & \vdots & \ddots & \vdots \\ -iN\omega m_n\omega_n & 0 & 0 & \cdots & m_n\left(-\omega^2+\omega_n^2\right) \end{vmatrix} = 0$$

Alternatively, we can also solve eq.(2.9) for q_{j0} and substitute this in eq.2.8, which results in the relation

$$\left(-m^*\omega^2 - eB_0\omega + m^*\omega_0^2\right) = N\sum_j^n m_j \frac{\omega^2\omega_j^2}{\left(-\omega^2+\omega_j^2\right)},$$

which, if we define the cyclotron frequency as $\omega_c = \frac{eB_0}{m^*}$, becomes

$$\left(-m^*\omega^2 - m^*\omega_c\omega + m^*\omega_0^2\right) = N\sum_j^n m_j \frac{\omega^2\omega_j^2}{\left(-\omega^2+\omega_j^2\right)}. \qquad (2.10)$$

Recall that this expression originated from the condition that our equations of motion be soluble. The allowed system frequencies can be found graphically by plotting the left versus right hand sides of this expression, and the intersections of these two curves give the solutions we seek. Alternatively, we can solve the above expression for ω, the system frequency. This gives us the dispersion relation, and plotting the roots of these expressions as functions of the field frequency, ω_j, gives us the dispersion diagram for the system. These will be shown in the Results section for a variety of cases.

Hamiltonian Treatment

Working from the Lagrangian (2.3) of the previous section, we can translate our results into Hamilton's formalism using the general prescription

$$H = \sum_{i=1}^{n} p_i \dot{q}_i - L,$$

where q_i is a general coordinate and p_i the corresponding conjugate momentum . In our case, the Hamiltonian becomes

$$H = \sum_{\alpha} \left(p_{z_\alpha} \dot{z}_\alpha + p_{z^*_\alpha} \dot{z}^*_\alpha \right) + \sum_{j} \left(p_{q_j} \dot{q}_j + p_{q^*_j} \dot{q}^*_j \right) - L. \tag{2.11}$$

The canonically conjugate momenta are given by $p_i = \frac{\partial L}{\partial \dot{q}_i}$ (see Appendix A), yielding

$$\begin{aligned}
p_{z_\alpha} &= \frac{\partial L}{\partial \dot{z}_\alpha} = \left\{ \frac{m^*}{2} \dot{z}^*_\alpha - \sum_j \frac{m_j \omega_j}{2} q^*_j + \frac{eB_0 i}{4} z^*_\alpha \right\}, \\
p_{z^*_\alpha} &= \frac{\partial L}{\partial \dot{z}^*_\alpha} = \left\{ \frac{m^*}{2} \dot{z}_\alpha - \sum_j \frac{m_j \omega_j}{2} q_j - \frac{eB_0 i}{4} z_\alpha \right\}, \\
p_{q_j} &= \frac{\partial L}{\partial \dot{q}_j} = \frac{m_j}{2} \dot{q}^*_j, \text{ and} \\
p_{q^*_j} &= \frac{\partial L}{\partial \dot{q}^*_j} = \frac{m_j}{2} \dot{q}_j
\end{aligned} \tag{2.12}$$

for the momenta conjugate to the coordinates z_α, z^*_α, q_j, and q^*_j, respectively. Substituting our conjugate momenta in eq.2.11, we find

$$\begin{aligned}
H &= \sum_{\alpha} \left\{ \frac{m^*}{2} \dot{z}^*_\alpha - \sum_j \frac{m_j \omega_j}{2} q^*_j + \frac{eB_0 i}{4} z^*_\alpha \right\} \dot{z}_\alpha \\
&\quad + \sum_{\alpha} \left\{ \frac{m^*}{2} \dot{z}_\alpha - \sum_j \frac{m_j \omega_j}{2} q_j - \frac{eB_0 i}{4} z_\alpha \right\} \dot{z}^*_\alpha \\
&\quad + \sum_j \frac{m_j}{2} \dot{q}^*_j \dot{q}_j + \sum_j \frac{m_j}{2} \dot{q}_j \dot{q}^*_j - L,
\end{aligned}$$

collecting terms and substituting eq.2.3 for the Lagrangian gives us

$$H(\dot{z}_\alpha, \dot{q}_i, z_\alpha, q_i) = \sum_\alpha \frac{m^*}{2}\left(\dot{z}_\alpha \dot{z}^*_\alpha + \omega_0^2 z_\alpha z^*_\alpha\right) + \sum_j \frac{m_j}{2}\left(\dot{q}_j \dot{q}^*_j + \omega_j^2 q_j q^*_j\right) + V_{coul}. \quad (2.13)$$

However, a Hamiltonian is properly a function of momenta and coordinates, that is $H = H\left(z_\alpha, p_{z_\alpha}, q_j, p_{q_j}\right)$, and the generalized velocities in eq.2.12 can be expressed in terms of the momenta p_{z_α} and p_{q_j} and their complex conjugates as

$$\begin{aligned}
\dot{z}^*_\alpha &= \frac{2}{m^*}\left(p_{z_\alpha} - \frac{eB_0 i}{4} z^*_\alpha + \sum_j \frac{m_j \omega_j}{2} q^*_j\right), \\
\dot{z}_\alpha &= \frac{2}{m^*}\left(p_{z^*_\alpha} + \frac{eB_0 i}{4} z_\alpha + \sum_j \frac{m_j \omega_j}{2} q_j\right), \\
\dot{q}^*_j &= \frac{2}{m_j} p_{q_j}, \text{ and} \\
\dot{q}_j &= \frac{2}{m_j} p_{q^*_j}. \qquad (2.14)
\end{aligned}$$

Substituting this in $H(\dot{z}_\alpha, \dot{q}_i, z_\alpha, q_i)$, we have

$$\begin{aligned}
H = \frac{m^*}{2}\frac{4}{(m^*)^2}&\left(\sum_\alpha p_{z^*_\alpha} + \frac{eB_0 i}{4}\sum_\alpha z_\alpha + \sum_j \frac{m_j\omega_j}{2} q_j\right) \\
&\cdot \left(\sum_\alpha p_{z_\alpha} - \frac{eB_0 i}{4}\sum_\alpha z^*_\alpha + \sum_j \frac{m_j\omega_j}{2} q^*_j\right) \\
&+ \sum_\alpha \frac{m^*}{2}\omega_0^2 z_\alpha z^*_\alpha + \sum_j \frac{2}{m_j}\left(p_{q_j} p^*_{q_j} + \frac{m_j^2\omega_j^2}{4} q_j q^*_j\right) + V_{coul}.
\end{aligned}$$

Expanding and collecting terms, along with the definition $\omega_c = \frac{eB_0}{m^*}$, gives us

$$\begin{aligned}
H = \frac{2}{m^*}&\left(\sum_\alpha p_{z^*_\alpha} p_{z_\alpha} + \sum_{\alpha j}\frac{m_j\omega_j}{2}\left(q_j p_{z_\alpha} + p_{z^*_\alpha} q^*_j\right) + \sum_j \frac{m_j^2\omega_j^2}{4} q_j q^*_j\right) + V_{coul} \\
&+ \sum_j\left(\frac{2}{m_j} p_{q^*_j} p_{q_j} + \frac{m_j\omega_j^2}{2} q_j q^*_j\right) + \sum_\alpha \frac{m^*\omega_0^2}{2} z_\alpha z^*_\alpha + i\frac{\omega_c}{2}\sum_\alpha\left(z^*_\alpha p_{z_\alpha} - p_{z^*_\alpha} z_\alpha\right) \\
&+ i\frac{\omega_c}{2}\sum_{\alpha j}\frac{m_j\omega_j}{2}\left(z_\alpha q^*_j - q_j z^*_\alpha\right) + \frac{m^*\omega_c^2}{2}\sum_\alpha z_\alpha z^*_\alpha, \qquad (2.15)
\end{aligned}$$

which is the Hamiltonian for the quantum dot-magnetic field system acted on by a homogenous time-varying electric field. Note that this is of the same form as the velocity coupling Hamiltonian discussed by Ford, Lewis, and O'Connell[4]. (With one exception: in a typical Hamiltonian we are accustomed to kinetic energy terms like $\frac{p^2}{2m}$. The Hamiltonian presented above, however, has kinetic energy terms that look like $\frac{2p^2}{m}$. This originates in the use of complex coordinates, and is explained in detail in appendix A.)

The External Field and the Centre of Mass

Returning to the Hamiltonian as a function of the coordinates and their generalized velocities, as in eq.2.13, we have

$$H(\dot{z}_\alpha, \dot{q}_i, z_\alpha, q_i) = \sum_\alpha \frac{m^*}{2}\left(\dot{z}_\alpha \dot{z}_\alpha^* + \omega_0^2 z_\alpha z_\alpha^*\right) + \sum_j \frac{m_j}{2}\left(\dot{q}_j \dot{q}_j^* + \omega_j^2 q_j q_j^*\right) + V_{coul}.$$

Making use of the complex version of the identity for quadratic forms[20]

$$\sum_\alpha^N (z_\alpha^* z_\alpha) = \frac{1}{N}\left(\sum_\alpha z_\alpha\right)^*\left(\sum_\alpha z_\alpha\right) + \frac{1}{N}\sum_{\alpha,\beta;\alpha<\beta}(z_\alpha - z_\beta)^*(z_\alpha - z_\beta),$$

we may recast the Hamiltonian in terms of centre of mass and relative motion coordinates for the electrons only, leaving the field terms as they are, resulting in

$$\begin{aligned} H \;=\; & \frac{m^*}{(2N)}\left(\sum_\alpha \dot{z}_\alpha\right)^*\left(\sum_\alpha \dot{z}_\alpha\right) + \frac{m^*}{(2N)}\sum_{\alpha,\beta;\alpha<\beta}(\dot{z}_\alpha - \dot{z}_\beta)^*(\dot{z}_\alpha - \dot{z}_\beta) \\ & + \frac{m^*\omega_0^2}{(2N)}\left(\sum_\alpha z_\alpha\right)^*\left(\sum_\alpha z_\alpha\right) + \frac{m^*\omega_0^2}{(2N)}\sum_{\alpha,\beta;\alpha<\beta}(z_\alpha - z_\beta)^*(z_\alpha - z_\beta) \\ & + \sum_j \frac{m_j}{2}\left(\dot{q}_j \dot{q}_j^* + \omega_j^2 q_j q_j^*\right) + e^2 \sum_{\alpha\neq\beta} \frac{1}{\sqrt{(z_\alpha - z_\beta)^*(z_\alpha - z_\beta)}}. \end{aligned} \tag{2.16}$$

We now redefine our coordinates to centre-of-mass and relative variables using the new coordinate definitions Z_{cm} for the electron centre of mass coordinate

$$Z_{cm} = \frac{1}{N}\sum_{\alpha}^{N} z_{\alpha},$$

and z_r for the electron relative motion coordinates

$$\begin{aligned}
z_{r_2} &= z_1 - z_2 \\
z_{r_3} &= z_1 + z_2 - 2z_3 \\
z_{r_4} &= z_1 + z_2 + z_3 - 3z_4 \\
&\vdots \\
z_{r_N} &= \sum_{\alpha=1}^{N-1} z_i - (N-1)\, z_N.
\end{aligned}$$

Likewise we can write the new electron velocity definitions $\dot{Z}_{cm}$ for the electron centre of mass velocity

$$\dot{Z}_{cm} = \frac{1}{N}\sum_{\alpha=1}^{N} \dot{z}_{\alpha},$$

and $\dot{z}_r$ for the electron relative motion velocity

$$\begin{aligned}
\dot{z}_{r_2} &= \dot{z}_1 - \dot{z}_2 \\
\dot{z}_{r_3} &= \dot{z}_1 + \dot{z}_2 - 2\dot{z}_3 \\
\dot{z}_{r_4} &= \dot{z}_1 + \dot{z}_2 + \dot{z}_3 - 3\dot{z}_4 \\
&\vdots \\
\dot{z}_{r_N} &= \sum_{\alpha=1}^{N-1} \dot{z}_i - (N-1)\, \dot{z}_N.
\end{aligned}$$

Our Hamiltonian expressed as a function of the centre of mass variables becomes

$$\begin{aligned} H &= \frac{(m^*N)}{2}\dot{Z}^*_{cm}\dot{Z}_{cm} + \frac{(Nm^*)}{2}\omega_0^2 Z^*_{cm}Z_{cm} \\ &+\frac{m^*}{(2N)}\sum_{\alpha,\beta;\alpha<\beta}(\dot{z}_\alpha - \dot{z}_\beta)^*(\dot{z}_\alpha - \dot{z}_\beta) + \frac{m^*\omega_0^2}{(2N)}\sum_{\alpha,\beta;\alpha<\beta}(z_\alpha - z_\beta)^*(z_\alpha - z_\beta) \\ &+\sum_j \frac{m_j}{2}\left(\dot{q}_j\dot{q}_j^* + \omega_j^2 q_j q_j^*\right) + e^2\sum_{\alpha\neq\beta}\frac{1}{\sqrt{(z_\alpha - z_\beta)^*(z_\alpha - z_\beta)}}. \end{aligned} \tag{2.17}$$

Inspection of this Hamiltonian reveals that each term is a function of either centre of mass coordinates or relative coordinates, but not both, and so may be written as a sum of centre of mass and relative Hamiltonians.

$$H\left(\dot{Z}_{cm}, \dot{z}_r, Z_{cm}, z_r, \dot{q}_j, q_j\right) = H_{cm}\left(\dot{Z}_{cm}, Z_{cm}\right) + H_r\left(\dot{z}_r, z_r\right) + H_{coul}\left(f(z_r)\right) + H_{field}(\dot{q}_j, q_j).$$

If we now consider the case where the dynamic vector potential, $\mathbf{A}_D$, is such that the electrons see an electric field which is slowly varying over the dimension of the quantum dot, i.e., $\mathbf{E}(\mathbf{r},t) = -e\mathbf{E}_0 e^{-i(\mathbf{k}\cdot\mathbf{r}-\omega t)} \approx \mathbf{E}(t) = -e\mathbf{E}_0 e^{-i\omega t}$, the interaction term in our Hamiltonian corresponding to the αth electron will be

$$H'_\alpha = -e\mathbf{E}_0 \cdot \mathbf{r}_\alpha e^{-i\omega t}.$$

(Note that this interaction is implicitly incorporated into our Hamiltonian (eq. 2.17) through the conjugate velocities that form the centre of mass terms. What we want to show here is the effect of this interaction Hamiltonian on the rest of eq. 2.17.)

The interaction term representing all of the electrons will be

$$H' = \sum_\alpha H'_\alpha$$

$$= \sum_{\alpha} \left(-e\mathbf{E}_0 \cdot \mathbf{r}_\alpha e^{-i\omega t}\right)$$
$$= \left(-e\mathbf{E}_0 e^{-i\omega t}\right) \cdot \sum_{\alpha} \mathbf{r}_\alpha.$$

Recalling that $\mathbf{R}_{cm} = \frac{1}{N}\sum_\alpha \mathbf{r}_\alpha$, this interaction term becomes

$$H' = (-Ne)\,\mathbf{E}_0 \cdot \mathbf{R}_{cm} e^{-i\omega t},$$

which we can write in terms of the complex coordinates if we first transform $\mathbf{E}_0$ to complex coordinates with the definitions $E_0 = E_{0x} + iE_{0y}$ and recall that $Z_{cm} = X_{cm} + iY_{cm}$. Then

$$\frac{(E_0 Z^*_{cm} + E^*_0 Z_{cm})}{2} = E_{0x}X_{cm} + E_{0y}Y_{cm} = \mathbf{E}_0 \cdot \mathbf{R}_{cm},$$

and the interaction Hamiltonian can now be written as

$$H' = (-Ne)\,\frac{(E_0 Z^*_{cm} + E^*_0 Z_{cm})}{2} e^{-i\omega t},$$

and so we see that the field interacts only with the centre-of-mass coordinates, and hence only the centre-of-mass Hamiltonian. This means that the electron-electron interactions do not play a role in the behavior of the centre of mass of the quantum dot–magnetic field–FIR field system.

For the case of FIR excitations the system dynamics are then represented exactly by the electron centre-of-mass Hamiltonian:

$$H_{cm}\left(\dot{Z}_{cm}, Z_{cm}, \dot{q}_j, q_j\right) = \frac{m^* N}{2}\dot{Z}^*_{cm}\dot{Z}_{cm} + \frac{(Nm^*)\,\omega_0^2}{2} Z^*_{cm} Z_{cm} + \sum_j^n \frac{m_j}{2}\left(\dot{q}_j\dot{q}^*_j + \omega_j^2 q_j q^*_j\right). \tag{2.18}$$

Which describes a collection of $n+1$ oscillators: one physical oscillator with mass Nm^* and charge Ne, and n field oscillators of effective mass m_j. Coupling of these oscillators occurs through the Z_{cm} and $\dot{Z}_{cm}$ terms.

Chapter 3

Results

From the preceding section we have as the solutions of the system the cyclic functions

$$Z_{cm}(t) = Z_0(\omega)\, e^{-i\omega t} \tag{3.1}$$

and

$$q_j(t) = q_{j0}(\omega)\, e^{-i\omega t}. \tag{3.2}$$

These can be identified with the Cartesian centre of mass coordinates in the usual way, namely $Z_{cm} = X_{cm} + iY_{cm}$. One can then write for Z_{cm}

$$X_{cm}+iY_{cm} = Z_0(\omega)\, e^{-i\omega t} = Z_0(\omega)\left[\cos(\omega t) - i\sin(\omega t)\right] = R\cos(\omega t+\phi) - iR\sin(\omega t+\phi),$$

and likewise for q_j. The system frequencies, ω, are determined from the solubility condition derived previously

$$\left(-\frac{m^*}{2}\omega^2 - \frac{m^*\omega_c}{2}\omega + \frac{m^*\omega_0^2}{2}\right) = N\sum_j^{n_j}\frac{m_j}{2}\frac{\omega^2\omega_j^2}{\left(\omega_j^2-\omega^2\right)}, \tag{3.3}$$

where n_j represents the number of field modes interacting with the electronic system, and N represents the number of electrons in the system. This expression is difficult to solve in its most general form, but with a few simplifications we can find analytic solutions for specific cases.

The Case of One Field Mode

If we specify only one field mode , $n_j = 1$, as would be the case for an ideal cavity, the summation drops out and our expression becomes

$$\left(-\omega^2 - \omega_c\omega + \omega_0^2\right)\left(\omega_j^2 - \omega^2\right) - N\frac{m_j}{m^*}\omega_j^2\omega^2 = 0,$$

or equivalently

$$\omega^4 + \omega_c\omega^3 - \left\{\omega_0^2 + \left(1 + N\frac{m_j}{m^*}\right)\omega_j^2\right\}\omega^2 - \omega_c\omega_j^2\omega + \omega_0^2\omega_j^2 = 0. \qquad (3.4)$$

We see that this is a quartic in ω, yielding four roots which we will label ω_1, ω_2, ω_3, and ω_4, the system frequencies. The solution of such a polynomial is fairly involved, and we will return to it later.

The Case of Zero Magnetic Field

The situation is greatly simplified in the case of zero magnetic field ($\omega_c = 0$), since the above equation becomes

$$\omega^4 - \left\{\omega_0^2 + \left(1 + N\frac{m_j}{m^*}\right)\omega_j^2\right\}\omega^2 + \omega_0^2\omega_j^2 = 0, \qquad (3.5)$$

a quartic whose four roots are the system frequencies we seek.

The Level Behavior

The quartic can easily be solved as a quadratic, and yields the roots (i.e., the dispersion relations)

$$\omega_1 = \frac{1}{2}\sqrt{\left(\omega_0^2+\omega_j^2+N\frac{m_j}{m^*}\omega_j^2+2\omega_0\omega_j\right)}+\frac{1}{2}\sqrt{\left(\omega_0^2+\omega_j^2+N\frac{m_j}{m^*}\omega_j^2-2\omega_0\omega_j\right)},$$

$$\omega_2 = \frac{1}{2}\sqrt{\left(\omega_0^2+\omega_j^2+N\frac{m_j}{m^*}\omega_j^2+2\omega_0\omega_j\right)}-\frac{1}{2}\sqrt{\left(\omega_0^2+\omega_j^2+N\frac{m_j}{m^*}\omega_j^2-2\omega_0\omega_j\right)},$$

$$\omega_3 = -\frac{1}{2}\sqrt{\left(\omega_0^2+\omega_j^2+N\frac{m_j}{m^*}\omega_j^2+2\omega_0\omega_j\right)}+\frac{1}{2}\sqrt{\left(\omega_0^2+\omega_j^2+N\frac{m_j}{m^*}\omega_j^2-2\omega_0\omega_j\right)},$$

and

$$\omega_4 = -\frac{1}{2}\sqrt{\left(\omega_0^2+\omega_j^2+N\frac{m_j}{m^*}\omega_j^2+2\omega_0\omega_j\right)}-\frac{1}{2}\sqrt{\left(\omega_0^2+\omega_j^2+N\frac{m_j}{m^*}\omega_j^2-2\omega_0\omega_j\right)}. \tag{3.6}$$

The behavior of these levels can best be demonstrated graphically, shown below in figure 1.

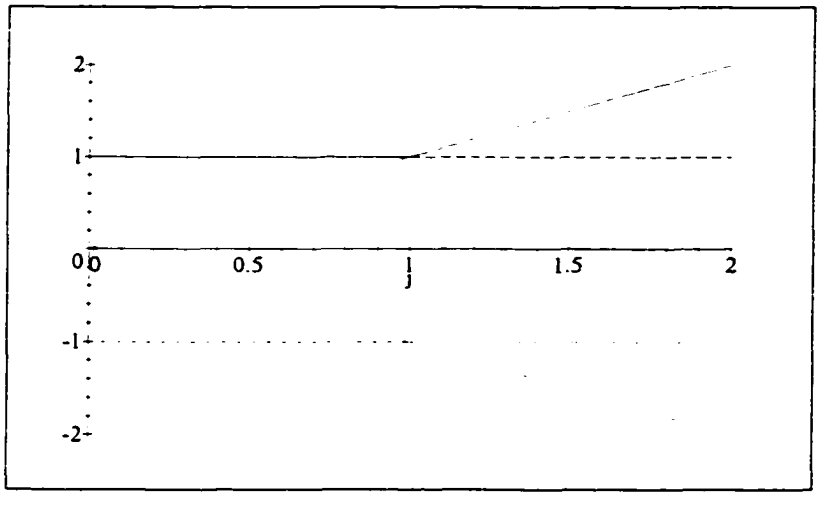

Figure 1. A plot of ω vrs. ω_j for one field mode. The levels exhibit anticrossing behavior when the field, ω_j, is resonant with the oscillator frequency, ω_0. The graph is plotted in terms of the variables $x = \frac{\omega}{\omega_0}$ and $j = \frac{\omega_j}{\omega_0}$, and so resonance occurs at $j = 1$. The coupling constant $N\frac{m_j}{m^*}\omega_j^2$ has been set at $.3 \times 10^{-8}$.

In plotting the curves shown in Figure 1, we have had to choose a numerical value for the quantity $N\frac{m_j}{m^*}$, which represents the degree of interaction between the electrons and the EM field, and hence may be thought of as a coupling constant. The behavior and evaluation of this coupling constant is treated in detail in the final section of this chapter. The anticrossing behavior of the levels may be easily seen at a finer scale, and expanding Figure 1 in the region where it exhibits anticrossing behavior yields the curves shown below in figure 2.

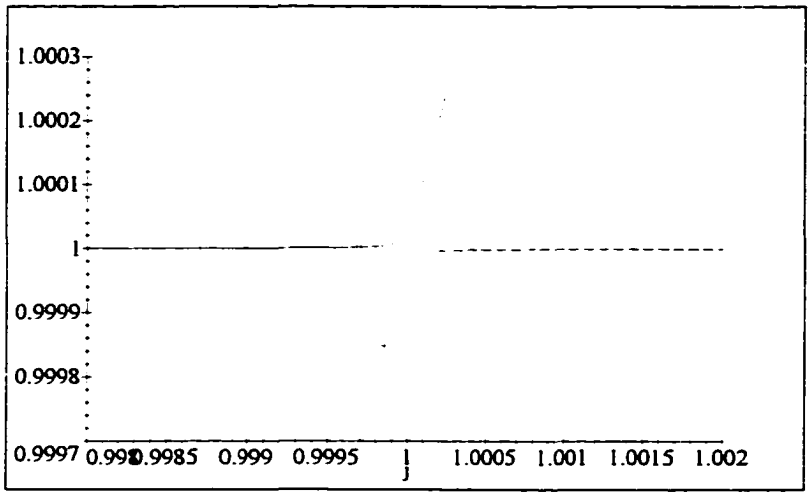

Figure 2. Detail of the anticrossing of levels ω_1 and ω_2. The vertical gap at resonance corresponds to the Rabi flopping energy.

Figure 2 shows the resonant anticrossing behavior of the system, and the splitting characteristic of Rabi oscillations as the system oscillates between an excited dot + ground state cavity and a ground state dot + excited cavity. The case we deal primarily with here, that of a single quantum dot occupied by one electron interacting with one field mode, is exactly the case of a dot in a resonant cavity.

The Graphical Solution

Note that we can also determine the system frequencies graphically. This involves independently plotting the left and right hand sides of the simplified solubility condition,

$$\frac{m^*}{2}\left(\omega_0^2-\omega^2\right)=N\frac{m_j}{2}\omega_j^2\frac{\omega^2}{\left(\omega_j^2-\omega^2\right)}. \tag{3.7}$$

The intersection of the resulting curves yield the solutions of the system. This graphical solution technique is familiar from the solutions of transcendental equations, and is the method employed by Ullersma[2] in his treatment of the Brownian motion problem and by Ford, Lewis and O'Connell[4] in their development of the quantum Langevin equation. The four intersections generated by our dispersion relation give the system frequencies, as shown below in figure 3.

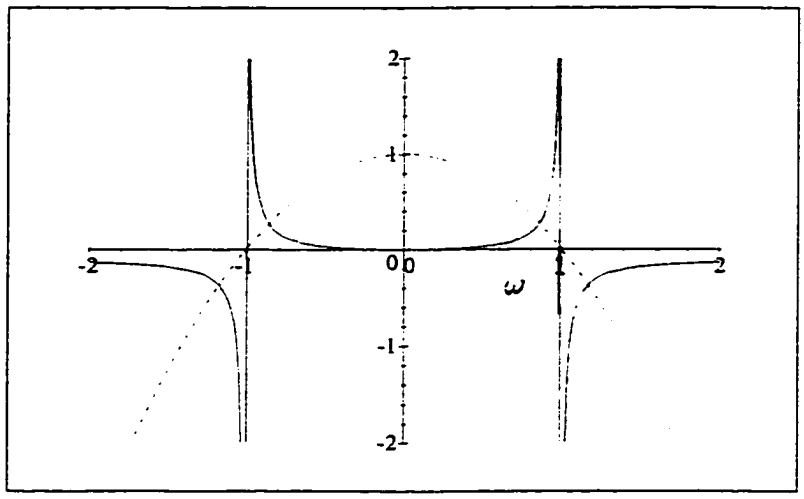

Figure 3. A plot of the LHS versus the RHS of the solubility condition for the case of no magnetic field. The intersections of the curves shown give the system

frequencies at resonance($\omega_j = \omega_0$). The coupling has been exaggerated for purposes of illustration.

In this simplified case of one field mode and zero magnetic field, this graphical solution technique is redundant since we already have an analytic expression for ω, but we will see that for the solution of more complex cases the technique proves very valuable.

The Case Involving a Magnetic Field

With only one field mode ($n_j = 1$) and a magnetic field present, the solubility condition becomes

$$\frac{m^*}{2}\left(\omega_0^2 - \omega_c\omega - \omega^2\right) = N\frac{m_j}{2}\omega_j^2\frac{\omega^2}{\left(\omega_j^2 - \omega^2\right)}.$$

Expanding this gives us the fourth-order polynomial

$$\omega^4 + \omega_c\omega^3 - \left\{\omega_0^2 + \left(1 + N\frac{m_j}{m^*}\right)\omega_j^2\right\}\omega^2 - \omega_c\omega_j^2\omega + \omega_0^2\omega_j^2 = 0,$$

which can be solved to give an analytic expression for the four system frequencies. We do this for the case we are most interested with: that where the electric field is resonant with the quantum dot potential, i.e. $\omega_j = \omega_0$, leaving ω_c independent. The quartic becomes

$$\omega^4 + \omega_c\omega^3 - \left\{\left(2 + N\frac{m_j}{m^*}\right)\omega_0^2\right\}\omega^2 - \omega_c\omega_0^2\omega + \omega_0^4 = 0, \tag{3.8}$$

and the roots of this expression give us the behavior of the levels with varying magnetic field.

The Level Behavior as a Function of Cyclotron Frequency

These roots are found using the standard algebraic solution formulae found in mathematical references. For quartics this can be a tedious process, and so here we have employed Maple, a software tool capable of analytic solutions of polynomials (up to fourth order). The roots generated in solving quartics can be extremely complicated, generally involving many terms. This was a limiting factor here, since in the most general case, where we wish to solve the quartic in terms of ω_j and ω_c, the roots generated were of a size that exceeded the capacities of the software to manipulate explicitly. This was not completely debilitating, however, since the dispersion curves could still be plotted implicitly, and explicit solutions were found for special cases, which we present below.

The case of fixed field frequency, $\omega_j = \omega_0$ (resonance), and variable cyclotron frequency, ω_c, was one such manageable case. The dispersions of the four system modes are given below, for the case of ten electrons and one field mode ($N = 10$ and $n_j = 1$, respectively).

$$\omega_1 = -.25\omega_c + 5.0 \times 10^{-5}\sqrt{(2.5 \times 10^7\omega_c^2 + 227.0)} + 5.0 \times 10^{-5}\sqrt{\left(-1.0\frac{-5.0\times10^7\omega_c^2\sqrt{(2.5\times10^7\omega_c^2+227.0)}-4.0\times10^8\sqrt{(2.5\times10^7\omega_c^2+227.0)}+2.5\times10^{11}\omega_c^3+2.27\times10^6\omega_c}{\sqrt{(2.5\times10^7\omega_c^2+227.0)}}\right)}$$

$$\omega_2 = -.25\omega_c + 5.0 \times 10^{-5}\sqrt{(2.5 \times 10^7\omega_c^2 + 227.0)} - 5.0 \times 10^{-5}\sqrt{\left(-1.0\frac{-5.0\times10^7\omega_c^2\sqrt{(2.5\times10^7\omega_c^2+227.0)}-4.0\times10^8\sqrt{(2.5\times10^7\omega_c^2+227.0)}+2.5\times10^{11}\omega_c^3+2.27\times10^6\omega_c}{\sqrt{(2.5\times10^7\omega_c^2+227.0)}}\right)}$$

$$\omega_3 = -.25\omega_c - 5.0\times10^{-5}\sqrt{(2.5\times10^7\omega_c^2+227.0)} + 5.0\times10^{-5}\sqrt{\left(\frac{5.0\times10^7\omega_c^2\sqrt{(2.5\times10^7\omega_c^2+227.0)}+4.0\times10^8\sqrt{(2.5\times10^7\omega_c^2+227.0)}+2.5\times10^{11}\omega_c^3+2.27\times10^6\omega_c}{\sqrt{(2.5\times10^7\omega_c^2+227.0)}}\right)},$$

and

$$\omega_4 = -.25\omega_c - 5.0\times10^{-5}\sqrt{(2.5\times10^7\omega_c^2+227.0)} - 5.0\times10^{-5}\sqrt{\left(\frac{5.0\times10^7\omega_c^2\sqrt{(2.5\times10^7\omega_c^2+227.0)}+4.0\times10^8\sqrt{(2.5\times10^7\omega_c^2+227.0)}+2.5\times10^{11}\omega_c^3+2.27\times10^6\omega_c}{\sqrt{(2.5\times10^7\omega_c^2+227.0)}}\right)}.$$

(3.9)

Plotting these yields the behavior shown below in figure 4.

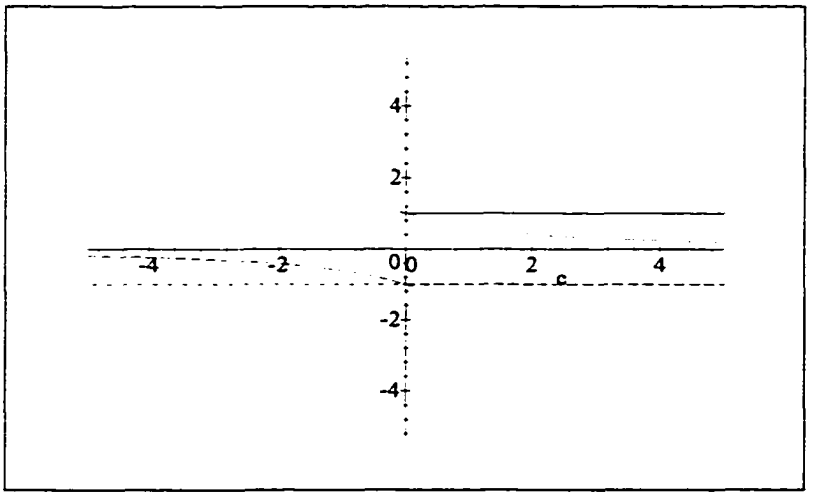

Figure 4a. A plot of the behavior of the levels with the field, ω_j, resonant with the oscillator frequency, ω_0, plotted as a function of the dimensionless variable c, where $c = \frac{\omega_c}{\omega_0}$ $\left(\omega_c = \frac{eB_0}{m^*}\right)$. The coupling constant is set at $\approx 3\times10^{-6}$.

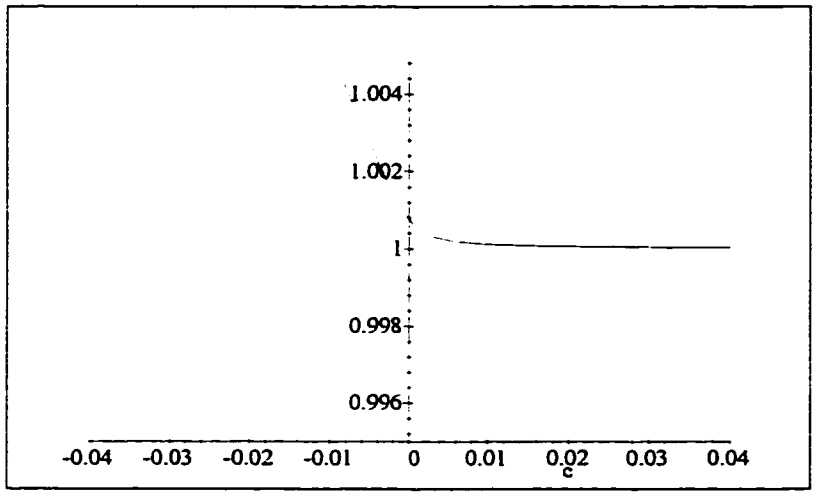

Figure 4b. An expanded plot of the positive frequency solutions from Figure 4a, showing the anticrossing behavior of the dot-cavity levels.

Recall that since the cyclotron frequency, ω_c, is defined as $\omega_c = \frac{eB_0}{m^*}$, and we have fixed the direction of $\mathbf{B}_0$, the sign change that occurs in the system frequencies $(\omega_1, ..., \omega_4)$ as they pass through zero represents a change in the rotation direction of the electron-field system. This is reflected in Figure 4a, since for any one solution the system displays asymmetric behavior with respect to ω_c, indicating that the magnetic field acts to increase or decrease the rotation frequency depending on the sign of ω_c and the handedness of the system solutions. Furthermore, each solution is seen to have a counterpart which exhibits antisymmetric behavior with respect to ω_c.

The Graphical Solution

We can apply the graphical intersection method to the case where the magnetic field is not zero, and once again a plot of the LHS and RHS of the dispersion relation,

$$\frac{m^*}{2}\left(\omega_0^2 - \omega_c\omega - \omega^2\right) = N\frac{m_j}{2}\omega_j^2\frac{\omega^2}{\left(\omega_j^2 - \omega^2\right)}, \tag{3.10}$$

yields the system frequencies from the four intersections of the given curves, shown below in figure 5. Again, a large coupling constant is used for illustration.

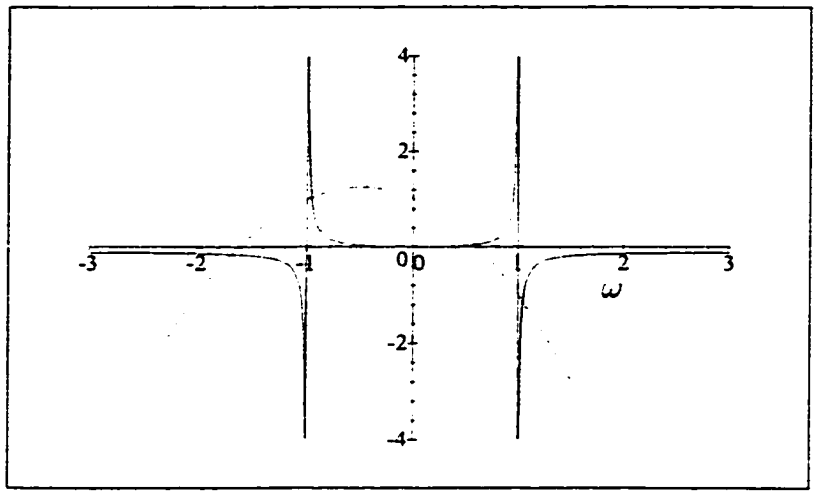

Figure 5. A plot of the system frequencies for the case of $\omega_c = \omega_0$. The magnetic field is seen to to shift the intersection points, and hence the system frequencies. Note that with a magnetic field present, we have lost the symmetry between positive and negative frequency solutions.

We can see that as the magnetic field increases in strength, the system frequencies grow smaller for positive ω, and larger for negative ω, corresponding to the cases where the circulation due to the magnetic field has a handedness opposite to

or the same as the handedness of the orbital motion of the composite electron centre of mass, respectively. This breaks the symmetry between the positive and negative frequency solutions for the dot, and allows us to distinguish each of the system modes individually. The explicit nature of this symmetry breaking can be discovered from a consideration of the magnetic dipole moment–magnetic field interaction energy, $U_B = -\mu \cdot \mathbf{B}$.

The magnetic dipole moment can be defined as

$$\mu = \frac{1}{2} \int_v (\mathbf{r} \times \mathbf{J})\, dv,$$

and so the interaction energy is

$$U_B = -\frac{1}{2} \left[\int_v (\mathbf{r} \times \mathbf{J})\, dv \right] \cdot \mathbf{B}.$$

where $\mathbf{J} = q\dot{\mathbf{r}} = -e\dot{\mathbf{r}}$ and $\mathbf{B} = B_0 \hat{\mathbf{z}}$. In the case of the quantum dot, both $\mathbf{r}$ and $\mathbf{J}$ lie in the x-y plane, so $\mathbf{r} \times \mathbf{J}$ will point either in the z or -z direction, parallel or antiparallel to the magnetic field. In the case where $\dot{\mathbf{r}}$ is oriented in a counterclockwise (ccw) direction, $\mathbf{J}$ is clockwise (cw), and so $\mathbf{r} \times \mathbf{J}$ points antiparallel to $\mathbf{B}$ which gives us $U_B = -\mu \cdot \mathbf{B} > 0$. Likewise, for $\dot{\mathbf{r}}$ oriented in a cw direction, $U_B = -\mu \cdot \mathbf{B} < 0$. If we now recall that $Z_{cm}(t) = X_{cm}(t) + iY_{cm}(t)$, which describes cw rotation for $\mathbf{Z}_{cm} \sim e^{-i\omega t}$ (see 3.1), we see that the case $U_B < 0$ corresponds to the Z_{cm} (or Z^*_{cm}) modes with $\omega > 0$ (or $\omega < 0$ for the Z^*_{cm} modes), decreasing (or increasing) the centre of mass rotation frequency as shown above in Figure 7. Likewise the $U_B > 0$ case corresponds to the Z^*_{cm} (or Z_{cm}) modes

with $\omega > 0$ (or $\omega < 0$ for the Z_{cm} modes), increasing (or decreasing) the centre of mass rotation frequency as also shown in Figure 7.

The Level Behavior as a Function of FIR Field Frequency

As mentioned above, explicit solutions for the system frequencies proved unmanageble owing to the length of the resulting expressions. This forced us to plot the dispersion curves implicitly, which are shown below in figure 6 in the case of a strong magnetic field ($\omega_c = \omega_0$) and an exaggerated coupling constant for purposes of illustration.

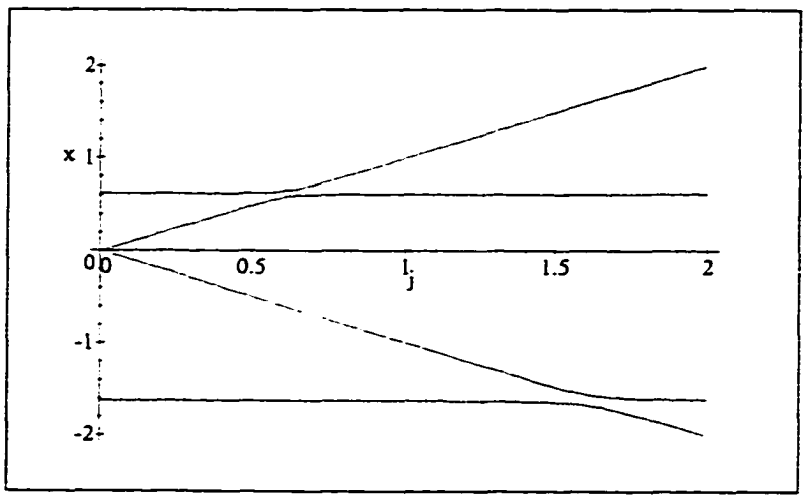

Figure 6. The system behavior for a dot in a strong magnetic field. Note how the magnetic field affects the Rabi frequency according to the sense of electronic centre-of-mass rotation.

The most notable effect of the magnetic field is to eliminate the degeneracy in the Rabi frequencies between the positive ($\omega > 0$) and negative ($\omega < 0$) frequency solutions. This implies that a quantum dot in a magnetic field discrim-

inates between left and right circularly polarized light, a fact which has been used extensively in the FIR characterizations of dots performed by the experimental community.

Multiple Field Modes

Returning to the situation where there are multiple field modes, we once again have our original solubility condition

$$\left(-\frac{m^*}{2}\omega^2 - \frac{m^*\omega_c}{2}\omega + \frac{m^*\omega_0^2}{2}\right) = N\sum_j^n \frac{m_j}{2}\frac{\omega^2\omega_j^2}{\left(\omega_j^2 - \omega^2\right)}. \tag{3.11}$$

With the summation present, it becomes increasingly difficult to find analytic solutions for the system frequencies, and so the graphical solution techniques of Ford, Lewis and O'Connell will be used to find the frequencies we seek.

The Case Without Magnetic Field

Exploring the simplest case first, consider the situation where there is no magnetic field. The solubility condition becomes

$$\left(-\frac{m^*}{2}\omega^2 + \frac{m^*}{2}\omega_0^2\right) = N\sum_j^n \frac{m_j}{2}\frac{\omega^2\omega_j^2}{\left(\omega_j^2 - \omega^2\right)},$$

which we rewrite for purposes of plotting as

$$\left(-\omega^2 + \omega_0^2\right) = N\sum_j^n \frac{m_j}{m^*}\frac{\omega^2\omega_j^2}{\left(\omega_j^2 - \omega^2\right)}. \tag{3.12}$$

Once again plotting the LHS and RHS we find the intersection points that give the system frequencies. This is shown below for the simplest case of two field

modes, $\omega_1 = \omega_0$ and $\omega_2 = 2\omega_0$.

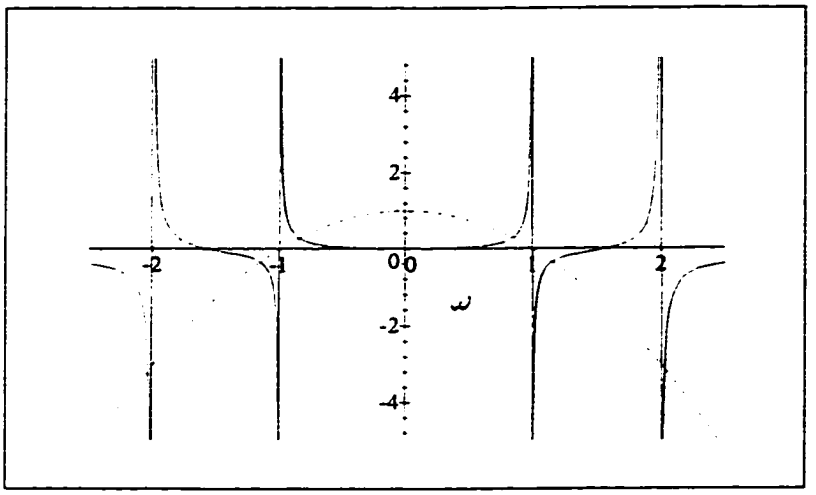

Figure 7. A plot of the system frequencies for a dot interacting with two field modes, $\omega_1 = \omega_0$ and $\omega_2 = 2\omega_0$. Note the appearance of two more system frequencies. The coupling constant here is set to 10^{-1}.

We can see that the number of solutions increases by two for each additional field mode, so for the case of two field modes we have the six system frequencies shown above. Furthermore, since the above plot is symmetrical, we can determine all the system frequencies by considering only the positive frequency ($\omega > 0$) solutions. This allows us to plot Figure 7 in the same manner as both Ullersma and Ford et. al., where we plot the LHS and RHS of the solubility condition as a function of ω^2 (labelled as v in Figure 8). This is shown below for purposes of comparison.

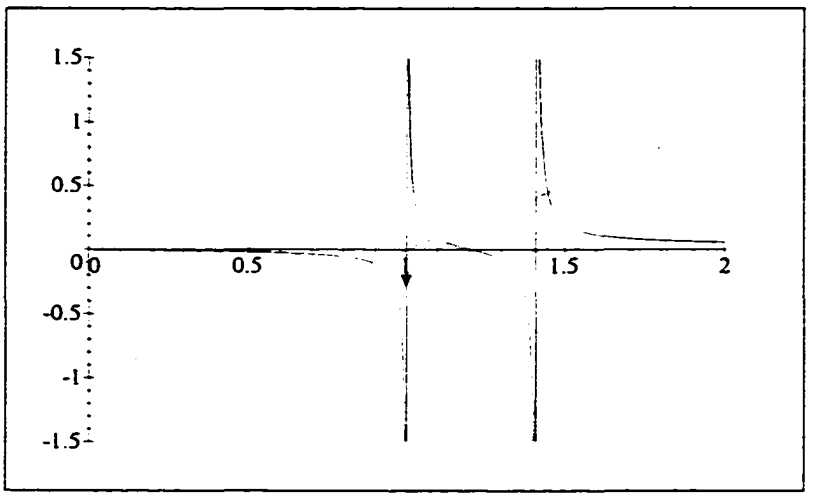

Figure 8. A plot of the system solutions in the style of Ullersma and Ford. The positive and negative roots of the intersection points shown above give the six system frequencies. The LHS and RHS of the dispersion relation are plotted as functions of ω^2, labelled as v in the graph.

The Case With Magnetic Field

If the magnetic field is now included in the system, the solubility condition becomes

$$\left(-\frac{m^*}{2}\omega^2 - \frac{m^*\omega_c}{2}\omega + \frac{m^*\omega_0^2}{2}\right) = N\sum_j^n \frac{m_j}{2}\frac{\omega^2\omega_j^2}{\left(\omega_j^2 - \omega^2\right)},$$

which we rewrite as

$$\left(-\omega^2 - \omega_c\omega + \omega_0^2\right) = \sum_j^n \frac{m_j}{m^*}\frac{\omega^2\omega_j^2}{\left(\omega_j^2 - \omega^2\right)} \tag{3.13}$$

and plot for the case of two field modes, $\omega_1 = \omega_0$ and $\omega_2 = 2\omega_0$, shown in figure 9.

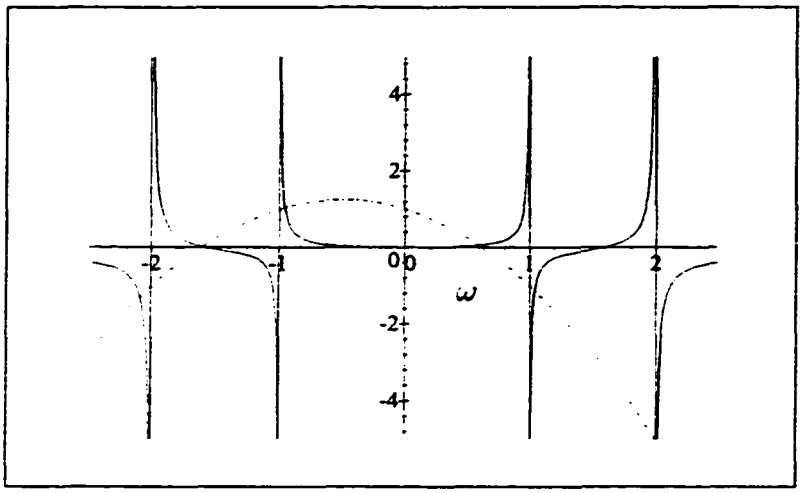

Figure 9. The case of a magnetic field and two field modes.

Note that in this case we are constrained to plot the LHS and RHS as functions of ω, since by including the magnetic field we have lost the symmetry of the previous ($B_0 = 0$) situation.

The Coupling Constant

If we consider the most general dispersion relation for our system,

$$\left(-\omega^2 - \omega_c\omega + \omega_0^2\right) = N\sum_j^{n_j} \frac{m_j}{m^*} \frac{\omega^2\omega_j^2}{\left(\omega_j^2 - \omega^2\right)}, \tag{3.14}$$

we can investigate the strength of the coupling of the electric field to the electrons in the system. Inspection of this dispersion relation indicates that the coupling of the electronic and field oscillators depends on the magnitude of the $N\sum_j \frac{m_j}{m^*}\omega_j^2$ term. With the definition of m_j given previously (and below) this simplifies to $\frac{e^2N}{\varepsilon m^* V}$. Since e, ε, and m^* are constants, we see that the coupling goes as $\frac{N}{V}$, the number of electrons divided by the cavity volume. This has two important

implications. First, that the strength of the coupling grows linearly as the number of electrons occupying a quantum dot. The $\frac{N}{V}$ dependance also indicates that the coupling grows linearly with the number of dots in the cavity volume, so long as the dots act as isolated entities, namely that they do not couple to each other (in practice this means an array of dots with a spacing large enough to ensure that there is no dipole interaction between adjacent dots). If we assume that each dot is occupied by the same number of electrons, the coupling constant will scale as $N_D N_e$, where N_D and N_e represent the number of dots and the number of electrons per dot, respectively. This assumption allows us to write the total number of electrons in the cavity as $N = N_D N_e$, which will be used for the calculated splitting of the oscillator levels presented below.

In the graphs of the preceding section the curves have been plotted against frequencies relative to the natural oscillator frequency, ω_0. This modifies the form of the dispersion relation slightly, and so a detailed treatment is presented here. As a matter of convenience we divide eq.3.14 through by ω_0^2 and introduce the dimensionless variables

$$x \equiv \frac{\omega}{\omega_0},\ j \equiv \frac{\omega_j}{\omega_0} \text{ and } \mathrm{c} \equiv \frac{\omega_c}{\omega_0}. \tag{3.15}$$

The dispersion relation then becomes

$$\left(-x^2 - cx + 1\right) = N \sum_j^{n_j} \frac{m_j}{m^*} j^2 \frac{x^2}{(j^2 - x^2)}, \tag{3.16}$$

and the strength of the particle-field coupling is determined solely by the coupling

constant, K, defined as

$$K = N\sum_{j}^{n_j} \frac{m_j}{m^*} j^2 \tag{3.17}$$

With the previous definition of m_j from Chapter 2, namely $m_j = \frac{e^2}{\varepsilon V \omega_j^2}$, and the definition $j \equiv \frac{\omega_j}{\omega_0}$, the coupling constant becomes

$$K = N\sum_{j} \frac{m_j}{m^*} j^2 = N\sum_{j} \frac{1}{m^*} \frac{e^2}{\varepsilon V \omega_j^2} \frac{\omega_j^2}{\omega_0^2} = \frac{Ne^2}{\varepsilon m^* \omega_0^2 V}.$$

Note that V in this expression is taken to be the volume occupied by the fundamental cavity mode, $\frac{\lambda_0}{2}$ (where $\lambda_0 \omega_0 = 2\pi c$), which for an idealized cubical resonator would be

$$V = \left(\frac{\lambda_0}{2}\right)^3.$$

The wavelength of this cavity mode can be expressed in terms of the oscillator frequency, ω_0, as

$$\lambda_0 = \frac{2\pi c}{n\omega_0},$$

where n is the index of refraction. This gives us for the volume of the fundamental cavity mode

$$V = \left(\frac{\lambda_0}{2}\right)^3 = \frac{\pi^3 c^3}{n^3 \omega_0^3},$$

and so our coupling constant becomes

$$K = \frac{Ne^2}{\varepsilon m^* \omega_0^2 V} = \frac{Ne^2}{\varepsilon m^* \omega_0^2} \cdot \frac{n^3 \omega_0^3}{\pi^3 c^3} = \frac{Nne^2}{\pi^3 \varepsilon_0 m^* c^3} \omega_0, \tag{3.18}$$

where we have used the relation between the index of refraction, n, and relative permittivity, $\varepsilon_r = n^2$. Note that because we have redefined our variables to x and

j, K is dimensionless. Values of the coupling constant K and the corresponding splitting of the normal modes are tabulated for a range of energies in Table 1 below for the case of a single electron dot ($N = 1$) in zero magnetic field, with $m^* = .069m_e$ and $\varepsilon_r = 12.65$ for GaAs.

ω_0 $(\frac{rad}{s})$	Energy	Range	$x_0 = \sqrt{\frac{\hbar}{m^*\omega_0}}$ (nm)	$K = 1.5 \times 10^{-22}\omega_0$	$\Delta\omega$ $\left(\frac{rad}{s}\right)$
6.09×10^9	$4\ \mu eV$	radio	459 nm	9.07×10^{-13}	6.69×10^3
1.53×10^{11}	$100\ \mu eV$	microwave	92 nm	2.28×10^{-11}	8.42×10^3
6.09×10^{11}	$400\ \mu eV$		46 nm	9.07×10^{-11}	6.69×10^6
1.17×10^{12}	$1.61\ meV$	far IR	33 nm	1.75×10^{-10}	1.78×10^7
1.53×10^{13}	$10\ meV$		9.15 nm	2.28×10^{-9}	8.42×10^8
6.13×10^{13}	$40.4\ meV$	mid IR	4.6 nm	9.14×10^{-9}	6.75×10^9
2.44×10^{14}	$161\ meV$		2.3 nm	3.63×10^{-8}	5.36×10^{10}
1.53×10^{15}	$1\ eV$	near IR	0.9 nm	2.28×10^{-7}	8.42×10^{11}
6.11×10^{15}	$4\ eV$	optical\uv	0.46 nm	9.12×10^{-7}	6.72×10^{12}

Table 1.

It is clear that the charge-field coupling scales linearly with the oscillator energy, and so the strongest coupling occurs for highly confined systems, and falls to zero for free systems, as expected. A comparison of K and $\Delta\omega$ in Table 1 above indicates that the magnitude of the splitting grows as $\sqrt{K}$, and hence as

$\sqrt{N} = \sqrt{N_D N_e}$, which can also be seen clearly in eq.3.6. For a realistic case N_e can be as large as 200 electrons, meaning splittings roughly 14 times larger than those stated in Table 1. N_D can also be quite large. Sikorski and Merkt use a dot spacing of 250 nm in a 3×3 mm^2 array for a total of $N_D = 1.44 \times 10^8$ non-interacting dots, and Reed et. al. use an array containing $N_D \approx 10^5$ non-interacting dots.

The values presented above for N_D and N_e indicate that large splittings should be observable for quantum dot arrays embedded in Bragg cavities. As an example, consider the entry in Table 1 where $\omega_0 = 1.53 \times 10^{15} \frac{rad}{s}$, yielding a splitting for a one-electron dot of $\Delta\omega = 8.42 \times 10^{11} \frac{rad}{s}$. If instead of a single dot we consider an array of 10^4 dots, each occupied by 100 electrons, the cavity induced splitting of the oscillator modes for $\omega_0 = 1.53 \times 10^{15} \frac{rad}{s}$ becomes $\Delta\omega = \sqrt{10^6} \cdot 8.42 \times 10^{11} \frac{rad}{s} = 8.42 \times 10^{14} \frac{rad}{s}$. Researchers in industry are currently attempting to find ways to embed dots in monolithic structures to facilitate their use in practical applications. As early as 1988 Reed et. al. used spun polyimide to fill dot arrays to allow the overlay of columnar dots with a conducting contact layer. Other groups have investigated the possibility of using semiconductor to fill arrays, with some success. If these groups achieve this goal, it may become possible to fabricate monolithic dot-cavity structures, which should demonstrate the behaviors presented here.

Chapter 4

Disscussion

The Centre of Mass Dynamics

We have found that an N-electron quantum dot interacting with a perpendicular magnetic field and a spatially homogenous electric field can be modelled as a single particle of mass Nm^* and charge Ne interacting with the those same fields, and that this system has exact solutions. This result stems from the applicability of Kohn's theorem to our system, yielding a system of coupled oscillators, which is solved exactly using techniques employed first by Ullersma and later by Ford, Lewis and O'Connell.

The behavior of this exact solution is investigated as a function of electric field frequency, ω_j, magnetic field strength, B_0, and number of field modes, n_j. We also investigate the strength of the coupling (K) between the electronic centre of mass oscillator and the field oscillators in terms of the system parameters.

An Exact Solution

The most notable aspect of the results presented here is that the solution is exact for the centre of mass behavior of our system. At first consideration

this may be somewhat surprising, since one would expect many-body interactions owing to the screened Coulombic potential existing between the electrons in the dot. Furthermore, since we deal here with the case of a two dimensional electron gas confined to a heterojunction, screening effects become weaker than in the three dimensional case and so we expect stronger interactions between electrons.

The system, originally envisioned as a quantum dot in a perpendicular magnetic field and illuminated with a spatially homogenous periodic electric field (i.e., assuming the dipole approximation), is modelled as a set of N electrons confined to a parabolic well and coupled to the electromagnetic field which itself is modelled as a family of harmonic oscillators. Note that if the electron-electron interaction term were not present in the above model, we would expect an exact solution, since a system of coupled oscillators possesses such solutions. What allows an exact solution in our case, with the electron-electron interactions present in the system, is that the electric field couples only to the centre of mass of the N electrons in the well and so the electron-electron interaction term (a function of relative coordinates) does not affect the centre of mass behavior of the system.

This independence of centre of mass and relative motion for a charged particle in a homogenous magnetic field and/or harmonic potential was established in 1961 with the by now well-known Kohn's Theorem[1], and applied more recently to quantum dots and parabolic quantum wells by Brey and Halperin[18] as the Generalized Kohn's Theorem (GKT). When the GKT is applied to our system,

we obtain the exact centre of mass solution presented in the thesis. This means that after a transformation to centre of mass and relative coordinates, we find that the dynamics of the centre of mass of the system are completely independent of the relative motion of the particles which comprise the system. Because the dot–field system can be modelled as a set of coupled harmonic oscillators, we can find an exact solution for the dynamics of the centre of mass. The solution for the relative motion dynamics of the system is naturally more complex and will generally require a numerical approach if more than a few particles are involved, since the electron-electron interactions must be incorporated into the calculation.

It is possible to make a clear distinction between those situations where the centre of mass solution will adequately describe the system dynamics and situations where the more detailed relative motion solutions are required for an adequate treatment of the system's behavior. In those cases where the incident electric field has a wavelength which is long in comparison with the dimensions of the dot, the centre of mass description will provide the system behavior. In those cases where the wavelength of the incident field approaches the dimensions of the dot, the solution for the relative motion of the particles is necessary to describe the behavior of the dot. Note that the absolute dimensions of the dot or the wavelength of the field are not important, what is important is the criteria that we are working in the dipole limit. This means that although the results presented here were originally motivated by an analysis of experimental FIR spectra

of quantum dots, they will in fact apply at larger and smaller length scales than are practically attainable with dots so long as we continue to work in the long wavelength (dipole) limit. As we have seen in Table 1 of the previous chapter , this becomes important since the magnitude of the splitting scales inversely with the physical dimensions of the system.

Comparison with the Atom-Cavity System

It is instructive to compare our dot-cavity system with another, more familiar, system – that of an atom in a confocal cavity. Experiments on these atom-cavity systems have yielded observations of vacuum field induced normal mode splitting (i.e., Rabi splitting) analogous with the splittings we have calculated for the quantum dot-cavity system. Because we have considered the splittings of a single dot-cavity system, the best example of the analogous atom-cavity system can be found in the work of Rempe, Thompson and Kimble[16] (RTK), who have studied the case of a single atom in a resonant confocal cavity and observed the Rabi splitting of an optical mode. A schematic of their experiment is shown below.

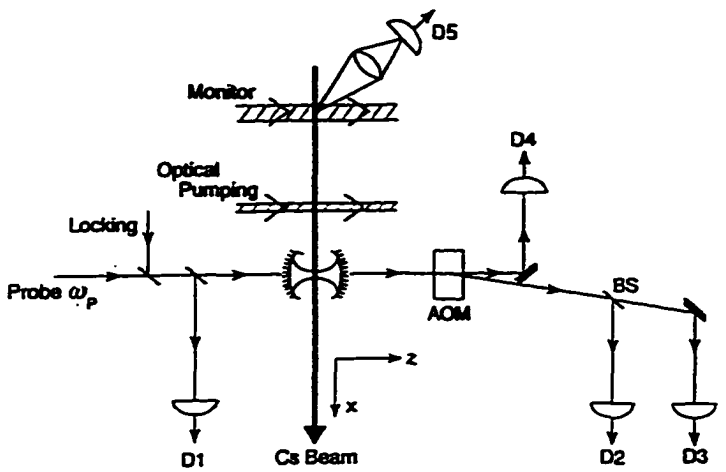

Fig. 1: Diagram of apparatus with atomic beam, monitor detector, optical pumping region, cavity and light detectors as described in the text.

Atom-Cavity Splitting

RTK consider the D_2 line of Cesium, produced by the $6S_{\frac{1}{2}}$, $F = 4$, $m_F = 4 \longleftrightarrow 6P_{\frac{3}{2}}$, $F' = 5$, $m_{F'} = 5$ transition. The D_2 line has a wavelength of 852 nm, with a corresponding frequency of 3.52×10^{14} Hz. They employ Cesium and laser beams of low atomic and photon number densities to ensure that on average only one atom and one photon occupy the confocal cavity, which has its resonance frequency tuned to the Cesium D_2 line. RTK use a standard analysis of this system, known as the Jaynes-Cummings model, which predicts Rabi oscillations between the atom and the single cavity mode. In their experimental setup, the laser beam (probe beam) is scanned through the atom-cavity resonance and the

transmission of the system as a function of the laser probe frequency is recorded. The splitting of the D_2 line yields the Rabi flopping frequency. Several examples of such splitting are shown below for varying mean number of intracavity atoms, $\bar{N}$.

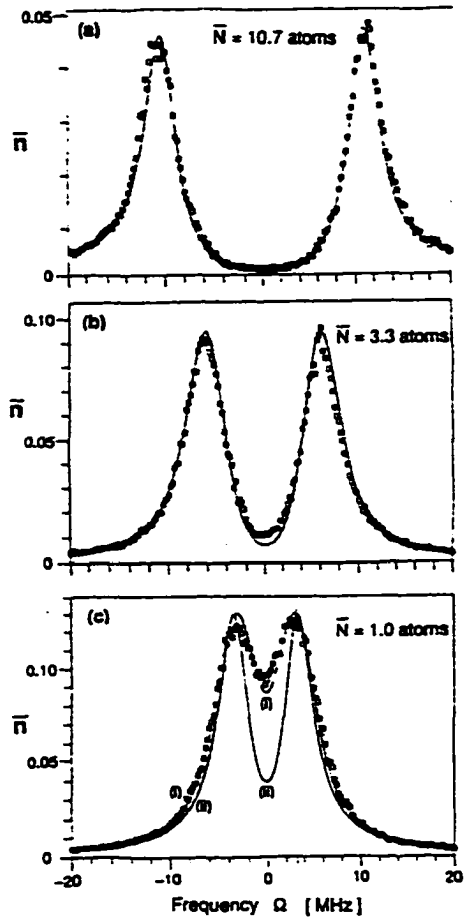

Fig. 2: Normal-mode or vacuum-Rabi splitting for different numbers of intracavity atoms. The transmitted intensity is plotted as a function of the detuning of the probe field Ω from the common atomic and cavity resonance frequency (ω_a=ω_c).

If we consider the case where on average only one atom occupies the cavity (i.e., $\bar{N}$=1), we find from the intensity versus frequency plots that the splitting frequency, Δf, is roughly 6 MHz. Compared to the unsplit D_2 line, this yields

a relative frequency splitting of $\frac{\Delta f}{f} = \frac{6\ MHz}{3.52\times 10^{14}\ Hz} = 1.71 \times 10^{-8}$. In terms of a percentage frequency shift, this is $\frac{\Delta f}{f}\% = 1.71 \times 10^{-6}\ \%$.

Dot-Cavity Splitting

The coupled oscillator analysis applied to the quantum dot-cavity system yields a splitting from the oscillator frequency given by the expression

$$\omega_1 = \frac{1}{2}\sqrt{\left(\omega_0^2 + \left(1 + N\frac{m_j}{m^*}\right)\omega_j^2 + 2\omega_0\omega_j\right)} + \frac{1}{2}\sqrt{\left(\omega_0^2 + \left(1 + N\frac{m_j}{m^*}\right)\omega_j^2 - 2\omega_0\omega_j\right)}.$$

If we evaluate this expression for a single-electron dot at the same resonance frequency and conditions as the atom-cavity system discussed above, that is $\omega_0 = 2\pi f = 2\pi\,(3.52 \times 10^{14}\ Hz) = 2.21 \times 10^{15}\ \frac{rad}{s}$ and $\omega_j = \omega_0$, we find a splitting frequency, $\Delta\omega$, of $\Delta\omega = 2\,(\omega_1 - \omega_0) = 4.4 \times 10^{7}\ \frac{rad}{s}$. This yields a relative splitting of $\frac{\Delta\omega}{\omega} = \frac{4.4\times 10^{7}\ \frac{rad}{s}}{2.21\times 10^{15}\ \frac{rad}{s}} = 2.0 \times 10^{-8}$, and a percentage splitting of $\frac{\Delta\omega}{\omega}\% = 2.0 \times 10^{-6}\%$. By comparison, this dot-cavity system displays roughly the same degree of splitting as the atom-cavity system. There is, however, one important difference between the dot and atom cavity systems, namely that in the dot-cavity case the splitting frequency scales as the square root of the number of electrons occupying the dot, that is as $\sqrt{N_e}\Delta\omega$, where $\Delta\omega$ is the splitting for a single-electron dot. The number of electrons which can occupy a dot is limited by the fact that as electrons are pushed into the dot, their Coulombic fields will distort the confinement potential until it is no longer parabolic. In practice, this number depends on the composition, design and physical dimensions of the dot. Demel[28]

et. al. have used as many as 210 electrons in a 600 nm radius dot, which would yield a splitting frequency approximately 14 times larger for the dot–cavity system than the corresponding atom–cavity system. This comparatively large splitting frequency could make the observation of vacuum-field induced Rabi oscillations possible for dot-cavity systems.

In addition to the $\sqrt{N_e}$ splitting with number of electrons per dot, the splitting will also scale as the square root of the number of dots in the cavity, $\sqrt{N_d}$, which means a total splitting of $\sqrt{N_d N_e}\Delta\omega$.

The question remains: can this predicted vacuum Rabi splitting be detected experimentally? To address this we consider several of the entries from Table 1 in the previous chapter, and express the peak splittings presented there in terms of conventional spectroscopic quantities.

$\omega\left(\frac{rad}{s}\right)$	*Range*	$\Delta\omega\left(\frac{rad}{s}\right)$	$\Delta\lambda$ (μm)	eV	*wavenumber* (cm^{-1})
1.17×10^{12}	*far IR*	1.78×10^{7}	1.06×10^{8}	11.7 neV	9.44×10^{-5}
1.53×10^{13}		8.42×10^{8}	2.24×10^{6}	0.55 μeV	4.47×10^{-3}
6.13×10^{13}	*mid IR*	6.75×10^{9}	2.79×10^{5}	4.44 μeV	3.58×10^{-2}
2.44×10^{14}		5.36×10^{10}	3.50×10^{4}	35.5 μeV	2.86×10^{-1}
1.53×10^{15}	*near IR*	8.42×10^{11}	2.24×10^{3}	0.55 meV	4.47

The wavenumbers presented above indicate that the vacuum induced Rabi

splitting of the oscillator modes is of a magnitude to allow detection with current equipment. Modern FTIR spectrometers have resolution on the order of 10^{-5} wavenumbers. Since the values in the table above can be scaled by the $\sqrt{N_d N_e}$ factor for numbers of dots and electrons, it seems that the effects presented in this thesis should be observable experimentally.

Coupled Oscillators or the RWA?

Note that we could also have modelled the dot-resonant cavity system with the well-known rotating wave approximation (RWA) of Jaynes and Cummings. This approximation consists essentially of discarding those elements of the particle-field interaction term that do not conserve energy, often called the virtual terms, and is frequently used in the field of quantum optics. The RWA can also be applied directly to our dot-resonant cavity system where the dot interacts with only one resonant cavity mode. For the case where only one quantum of energy inhabits the system the dot will be in either its ground or first excited state, and so can be viewed as a two-state atom and treated by the RWA, which yields well-known analytic solutions. It becomes apparent that our dot-cavity system can be modelled either as coupled oscillators or as a two-state atom interacting with the EM field in the rotating wave approximation. A comparison of the properties of these respective solutions shows the coupled-oscillator model to be the preferable choice for the dot-cavity system, and also the preferable choice for several other

systems which are frequently modelled using the RWA.

The most obvious advantage of the oscillator solution is that it is exact for all frequencies, whereas the RWA solution applies only near resonance. Extending the RWA solution to ensure its validity off-resonance requires the use of perturbation theory, which can lead to questions concerning the convergence of the perturbation expansion.

Ford, Lewis and O'Connell make the point that the RWA is a version of the linear-coupling model of a heat bath, which has the flaw characterizing all such linear coupling models: that the lowest frequency solution of the system is imaginary, and so the ground state energy of the bath becomes increasingly negative as time passes (the solution is a growing exponential), i.e., the bath is not passive. Correcting the RWA with the electron's self-interaction terms cures this behavior and results in a physically realistic passive bath. FLO'C show that this corrected RWA is exactly equivalent to the independent oscillator (IO) model of the bath, and so in the end nothing is gained by the use of the RWA. (The one exception to the usefulness of the RWA is in the treatment of those systems which are genuine two-state entities, such as spin systems. In this case the two-state atom and the RWA are a realistic model of the system.)

Rabi is well-known for his work on such a two-state system, namely a spin-$\frac{1}{2}$ magnetic dipole interacting with a resonant radio field. The periodic exchange of energy that arises is such systems now bears the title of Rabi oscillations. The

two-state atom (TSA) interacting with an electric field is also an example of a system that exhibits these oscillations, and in 1963 Jaynes and Cummings were the first to apply the RWA to the two-state atom in the special case where only one (optical) resonant cavity mode interacts with the TSA. Tavis and Cummings in 1968 worked out the theory for the case where N two-state atoms interact with a single resonant cavity mode. Because of the technical challenge of setting up an atomic Rabi system in the real world, experiment has lagged theory throughout the history of the topic. The original experiment performed by Rabi and his collaborators in 1936 was a Stern-Gerlach type experiment, in which they performed radio spectroscopy on molecular and atomic beams. Measurements at microwave frequencies were originally made on a large collection of atoms in 1983, and similar work was done in the optical domain in 1986. The case originally described by Jaynes and Cummings proved to be the most challenging experimentally, and was not performed successfully until 1993, a thirty year gap between theory and experiment.

Although the theory of Rabi oscillations was originally developed to describe the interaction of atomic (or molecular beams) with a resonant electric field, recent exciting developments in device physics have lead to this phenomena being observed in the solid state. Weisbuch et. al. have recently (1992) demonstrated the existence of Rabi oscillations for quantum well excitons in a semiconductor heterojunction embedded within a DBR cavity.

The work presented here predicts vacuum Rabi splitting for a quantum dot in a cavity, and in this sense we have come full circle: dots have become known as artificial atoms (the number of electrons in a dot determines which "element" we have), and dots placed in proximity to other dots will couple and produce an artificial molecule. These artificial atoms and molecules will interact with the EM field and in the proper circumstances, manifest Rabi oscillations of their own.

Extending the Model

The model we present here yields useful information on several aspects of the dot-field behavior. Of primary interest in this thesis was the dispersion behavior of the system. In the course of determining the dispersion relations we also found the classical equations of motion and explicitly determined the form of the coupling constant. Other information can be extracted from the coupled oscillator model, for example one could calculate the lifetimes of excited isolated dots using Fermi's Golden Rule to determine the rate at which the excited dot loses energy to the continuum of available EM field states.

The system as it stands could also be quantized with the appropriate set of commutation relations, although for our purposes this was unnecessary since the dispersion relation is unchanged in the quantum limit. A quantized treatment would allow a calculation of the oscillator strength matrix elements which would in turn yield the intensity profile for the dot-field spectrum. One could also use

a second quantized treatment to express the system in terms of its oscillator and field creation and annihilation operators.

While the model used here is adequate for our purposes, a more realistic model will eventually be needed to accurately predict the behavior of real-world dots. This can be accomplished with a more sophisticated coupled oscillator model. Some of the necessary modifications are discussed below.

In this thesis we have modelled the dot–EM field system as a collection of coupled oscillators. These oscillators were assumed to be ideal, suffering no frictional forces or other dissipative losses. This is an approximation, of course, and since the majority of real systems will display some degree of dissipation, an improved oscillator model of such systems should take account of these losses. In classical mechanics this is accomplished through the use of a damping term, which can be either derived (as in the case of the viscous damping force described by Stoke's Law) or determined phenomenologically by comparing experimental data to the general solution for a damped oscillator. Our system consists of the centre of mass electron oscillator coupled to a (family of) cavity–field oscillator(s), each of which will be subject to various damping mechanisms.

Consider first the electron oscillator. Any mechanism by which the electron can lose energy other than radiating it into the cavity–field oscillator mode will constitute a dissipative process as far as Rabi oscillations are concerned. Scattering from impurities in the semiconductor crystal, interactions with phonons,

interaction with defect states at the heterojunction interfaces, radiation into field modes other than the desired cavity–field oscillator modes and trapping in dangling bonds resulting from the etching process are all possible sources of dissipation in semiconductor quantum dot devices. If these processes could be modeled explicitly in terms of the electron centre of mass position and momenta coordinates, it might be possible to explicitly derive a damping term that reproduces the phenomenological damping constant.

Likewise, we can consider the cavity–field oscillator. Both confocal and distributed Bragg reflector cavities are characterized by how quickly the cavity decays from its excited resonant mode to its unexcited state. The speed of this decay is determined by factors such as the geometry of the cavity, the absorptivity of any media inside the cavity, and the reflectivity of the cavity mirrors. Again, it may be possible to derive an effective decay constant based on an analysis of these dissipative mechanisms, and compare this derived constant to its experimentally determined value.

With acceptable values for the particle and cavity–field oscillator decay constants, one could then solve the resulting system of coupled damped oscillators. This would be a significant improvement over the work presented in this thesis, providing not only the system frequencies, but also the linewidths of these frequencies, allowing a complete prediction of the quantum dot–cavity field spectra.

Appendices

A. Complex Coordinates

In this thesis we have made use of complex coordinates in order to write a Lagrangian (originally expressed in terms of real displacement and velocity vectors) as a real function of complex coordinates. This is motivated by the circular symmetry of our quantum dot-magnetic field system. The resulting Lagrangian is easier to work with since terms originally containing inner products become terms containing only complex multiplication.

The change of coordinates from real vectors to complex scalars is straightforward. We begin with the real Lagrangian

$$L = \sum_{\alpha} \frac{m}{2}\left(\dot{\mathbf{r}}_{\alpha}^2 - \omega_0^2 \mathbf{r}_{\alpha}^2\right) - V_{coul} + \sum_{j} \frac{m_j}{2}\left[\dot{\mathbf{q}}_j^2 - \omega_j^2 \mathbf{q}_j^2\right] - \sum_{\alpha,j} m_j \omega_j \dot{\mathbf{r}}_{\alpha} \cdot \mathbf{q}_j - e \sum_{\alpha} \dot{\mathbf{r}}_{\alpha} \cdot \mathbf{A}_s$$

and define the complex coordinates $z_\alpha = x_\alpha + iy_\alpha$ and $q_j = q_{x_j} + iq_{y_j}$ for the particle and field displacements, respectively. Various linear combinations of these coordinates (and their time derivatives, $\dot{z}_\alpha = \dot{x}_\alpha + i\dot{y}_\alpha$ and $\dot{q}_j = \dot{q}_{x_j} + i\dot{q}_{y_j}$) give us

the terms in the new Lagrangian. These combinations are

$$\begin{aligned}
\dot{\mathbf{r}}_\alpha^2 &= \dot{x}_\alpha^2 + \dot{y}_\alpha^2 = \dot{z}_\alpha \dot{z}_\alpha^*, \\
\mathbf{r}_\alpha^2 &= x_\alpha^2 + y_\alpha^2 = z_\alpha z_\alpha^*, \\
\dot{\mathbf{q}}_j^2 &= \dot{q}_{x_j}^2 + \dot{q}_{y_j}^2 = \dot{q}_j \dot{q}_j^*, \\
\mathbf{q}_j^2 &= q_{x_j}^2 + q_{y_j}^2 = q_j q_j^*, \\
\dot{\mathbf{r}}_\alpha \cdot \mathbf{q}_j &= \dot{x}_\alpha q_{x_j} + \dot{y}_\alpha q_{y_j} = \dot{z}_\alpha q_j^* + \dot{z}_\alpha^* q_j.
\end{aligned} \tag{A.1}$$

Finally, we can also express the Coulomb term in complex coordinates

$$V_{coul} = \sum_{\alpha,\beta} \frac{e^2}{|\mathbf{r}_\alpha - \mathbf{r}_\beta|} = \sum_{\alpha,\beta} \frac{e^2}{\sqrt{\left(z_\alpha^* - z_\beta^*\right)\left(z_\alpha - z_\beta\right)}}. \tag{A.2}$$

These allow us to write our Lagrangian as

$$\begin{aligned}
L &= \sum_\alpha \frac{m}{2}\left(\dot{z}_\alpha \dot{z}_\alpha^* - \omega_0^2 z_\alpha z_\alpha^*\right) - V_{coul} + \sum_j \frac{m_j}{2}\left[\dot{q}_j \dot{q}_j^* - \omega_j^2 q_j q_j^*\right] \\
&\quad - \sum_{\alpha,j} \frac{m_j \omega_j}{2}\left(\dot{z}_\alpha q_j^* + \dot{z}_\alpha^* q_j\right) - e\sum_\alpha \dot{\mathbf{r}}_\alpha \cdot \mathbf{A}_s,
\end{aligned}$$

leaving only the $e\sum_\alpha \dot{\mathbf{r}}_\alpha \cdot \mathbf{A}_s$ term in real coordinates. This can be remedied through choosing a specific form for $\mathbf{A}_s$, namely $\mathbf{A}_s = \frac{B_0}{2}(-y, x, 0)$, a constant magnetic field in the z direction, perpendicular to plane inhabited by the electrons. The Lagrangian then becomes

$$\begin{aligned}
L &= \sum_\alpha \frac{m}{2}\left(\dot{z}_\alpha \dot{z}_\alpha^* - \omega_0^2 z_\alpha z_\alpha^*\right) - V_{coul} + \sum_j \frac{m_j}{2}\left[\dot{q}_j \dot{q}_j^* - \omega_j^2 q_j q_j^*\right] \\
&\quad - \sum_{\alpha,j} \frac{m_j \omega_j}{2}\left(\dot{z}_\alpha q_j^* + \dot{z}_\alpha^* q_j\right) - \frac{eB_0 i}{4}\sum_\alpha \left(z_\alpha \dot{z}_\alpha^* - z_\alpha^* \dot{z}_\alpha\right),
\end{aligned} \tag{A.3}$$

and so we have written the Lagrangian as a real function of complex coordinates. Note that although L is a function of complex variables, it does not satisfy the

Cauchy-Riemann equations. This means that L is not analytic on the complex plane. As an example, consider the function $f = zz^* = \mathrm{r}_\alpha^2 = x^2 + y^2$. If we express f as an arbitrary complex number, say $f = u + iv$, we have $u = x^2 + y^2$ and $v = 0$. The Cauchy-Riemann equations,

$$\begin{aligned} \frac{\partial u}{\partial x} &= \frac{\partial v}{\partial y} \\ \frac{\partial u}{\partial y} &= -\frac{\partial v}{\partial x}, \end{aligned}$$

applied to $f = zz^*$, yield

$$\frac{\partial u}{\partial x} = 2x \neq \frac{\partial v}{\partial y} = 0$$

and

$$\frac{\partial u}{\partial y} = 2y \neq -\frac{\partial v}{\partial x} = 0,$$

which tells us that f is not analytic on the complex plane, except in the trivial case where $x = y = 0$. This same argument holds for our Lagrangian, L.

The solution of the system now requires that we develop the equations of motion for the system, which we find from Lagrange's equation:

$$\frac{d}{dt}\left(\frac{\partial L}{\partial \dot{x}_i}\right) - \frac{\partial L}{\partial x_i} = 0,$$

where x_i represents the dynamical variables of the system. In our case, these dynamical variables are z_α, z_α^*, q_j, and q_j^*, which means that we will need to evaluate partial derivatives like $\frac{\partial L}{\partial z_\alpha}$ and $\frac{\partial L}{\partial q_j}$. But what does a partial derivative with respect to these complex coordinates mean? We can get a feeling for this by

considering a function $f(x,y)$, and operating on f with $\frac{\partial}{\partial z}$ using the formal rules of calculus. The chain rule gives us

$$\frac{\partial f(x,y)}{\partial z} = \frac{\partial f}{\partial x}\frac{\partial x}{\partial z} + \frac{\partial f}{\partial y}\frac{\partial y}{\partial z},$$

which we can evaluate using our original definitions of the complex coordinates. If $z = x + iy$, then we can write x and y as linear combinations of z and z^*. These are

$$x = \frac{(z+z^*)}{2} \text{ and } y = \frac{-i(z-z^*)}{2}, \tag{A.4}$$

from which we see that

$$\frac{\partial x}{\partial z} = \frac{\partial}{\partial z}\frac{(z+z^*)}{2} = \frac{1}{2} \text{ and } \frac{\partial y}{\partial z} = \frac{\partial}{\partial z}\frac{-i(z-z^*)}{2} = \frac{-i}{2}.$$

Substituting these into $\frac{\partial f(x,y)}{\partial z}$, we get

$$\frac{\partial f(x,y)}{\partial z} = \frac{1}{2}\left(\frac{\partial f}{\partial x} - i\frac{\partial f}{\partial y}\right).$$

from which we surmise the form of the operator $\frac{\partial}{\partial z_\alpha}$ to be

$$\frac{\partial}{\partial z_\alpha} = \frac{1}{2}\left(\frac{\partial}{\partial x_\alpha} - i\frac{\partial}{\partial y_\alpha}\right). \tag{A.5}$$

Likewise, we find

$$\frac{\partial}{\partial z_\alpha^*} = \frac{1}{2}\left(\frac{\partial}{\partial x_\alpha} + i\frac{\partial}{\partial y_\alpha}\right), \tag{A.6}$$

$$\frac{\partial}{\partial q_j} = \frac{1}{2}\left(\frac{\partial}{\partial q_{x_j}} - i\frac{\partial}{\partial q_{y_j}}\right), \tag{A.7}$$

and

$$\frac{\partial}{\partial q_j^*} = \frac{1}{2}\left(\frac{\partial}{\partial q_{x_j}} + i\frac{\partial}{\partial q_{y_j}}\right) \tag{A.8}$$

for the forms of the other complex differential operators.

In an identical manner, we can also determine the form of differential operators such as $\frac{\partial}{\partial \dot{z}_\alpha}$. These are

$$\frac{\partial}{\partial \dot{z}_\alpha} = \frac{1}{2}\left(\frac{\partial}{\partial \dot{x}_\alpha} - i\frac{\partial}{\partial \dot{y}_\alpha}\right), \tag{A.9}$$

and

$$\frac{\partial}{\partial \dot{q}_j} = \frac{1}{2}\left(\frac{\partial}{\partial \dot{q}_{x_j}} - i\frac{\partial}{\partial \dot{q}_{y_j}}\right)$$

and likewise for the complex congujate operators.

With these in hand, we can proceed to find the equations of motion from the Lagrangian of our system in the normal way, performing the complex derivatives in manner prescribed by the above complex differential operators.

It is important to note that employing complex coordinates will change the form of the Lagrangian and Hamiltonian functions. Compare the familiar real Hamiltonian for a free particle,

$$H\left(\mathrm{r}_\alpha, \mathrm{p}_{r_\alpha}\right) = \frac{p_{r_\alpha}^2}{2m},$$

to the complex Hamiltonian for the same free particle

$$H\left(z_\alpha, p_{z_\alpha}\right) = \frac{2p_{z_\alpha}^2}{m}.$$

The apparent factor of four difference between the two Hamiltonians stems from the definitions of momentum in the real and complex planes. In the real plane we

have

$$\mathbf{p}_{r_\alpha}^2 = p_{x_\alpha}^2 + p_{y_\alpha}^2,$$

with p_{x_α} and p_{y_α} given by

$$p_{x_\alpha} = \frac{\partial}{\partial \dot{x}_\alpha} L \text{ and } p_y = \frac{\partial}{\partial \dot{y}_\alpha} L,$$

or, expressing these momenta as differential operators, we find

$$p_{x_\alpha} = \frac{\partial}{\partial \dot{x}_\alpha} \text{ and } p_{y_\alpha} = \frac{\partial}{\partial \dot{y}_\alpha}.$$

In the complex plane the same development yields

$$p_{z_\alpha}^2 = p_{z_\alpha} p_{z_\alpha}^*,$$

with p_{z_α} and $p_{z_\alpha}^*$ given by

$$p_{z_\alpha} = \frac{\partial}{\partial \dot{z}_\alpha} L \text{ and } p_{z_\alpha}^* = \frac{\partial}{\partial \dot{z}_\alpha^*} L,$$

or, in operator form

$$p_{z_\alpha} = \frac{\partial}{\partial \dot{z}_\alpha} \text{and } p_{z_\alpha}^* = \frac{\partial}{\partial \dot{z}_\alpha^*}.$$

These complex differential momentum operators can be written explicitly based on equation A.9 and its complex conjugate,

$$p_{z_\alpha} = \frac{\partial}{\partial \dot{z}_\alpha} = \frac{1}{2}\left(\frac{\partial}{\partial \dot{x}_\alpha} - i\frac{\partial}{\partial \dot{y}_\alpha}\right) \text{ and } p_{z_\alpha}^* = \frac{\partial}{\partial \dot{z}_\alpha^*} = \frac{1}{2}\left(\frac{\partial}{\partial \dot{x}_\alpha} + i\frac{\partial}{\partial \dot{y}_\alpha}\right),$$

from which we can see that

$$p_{z_\alpha} = \frac{1}{2}\left(p_{x_\alpha} - i p_{y_\alpha}\right) \text{ and } p_{z_\alpha}^* = \frac{1}{2}\left(p_{x_\alpha} + i p_{y_\alpha}\right).$$

Returning to the complex Hamiltonian, we have

$$H(z_\alpha, p_{z_\alpha}) = \frac{2p_{z_\alpha}^2}{m} = \frac{2}{m} \cdot \frac{1}{2}\left(\frac{\partial}{\partial \dot{x}_\alpha} - i\frac{\partial}{\partial \dot{y}_\alpha}\right) \cdot \frac{1}{2}\left(\frac{\partial}{\partial \dot{x}_\alpha} + i\frac{\partial}{\partial \dot{y}_\alpha}\right) = \frac{p_{r_\alpha}^2}{2m},$$

and so the real and complex Hamiltonians can be seen to be equivalent. The factor of four difference stems from the use of complex coordinates.

In the course of our change of variables from real vector to complex scalar coordinates, we also encounter some complication when the degrees of freedom of the system are considered. Where we began with two degrees of freedom labelled by r and q, we now apparently have four degrees of freedom, labelled by z_α, z_α^*, q_j, and q_j^*. The situation resolves itself when we realize that the equations of motion in the case of the complex coordinates are redundant, since the equation of motion for z_α is simply the complex conjugate of that for z_α^*, and likewise for q_j and q_j^*.

B. Kohn's Theorem

The use of Kohn's theorem[1] is essential to the investigation of the behavior of a quantum dot immersed in a magnetic field interacting with a spatially homogenous, time-varying electric field. The theorem is simply stated: given an electron gas in a constant magnetic field, the cyclotron resonance frequency of the system is independent of the electron-electron interaction. More recent and slightly more general incarnations of the theorem are known as the generalized Kohn's theorem (GKT)(Brey[18] et. al., 1989; S.K. Yip[20], 1990) or the Harmonic Potential

theorem (HPT)(Dobson[19], 1994).

Both GKT and HPT (which is itself an extension of GKT) differ from the original Kohn's theorem in that they allow for an external scalar harmonic potential (most generally, $V_{ext} = \frac{m^*}{2}\left(\omega_x^2 x^2 + \omega_y^2 y^2 + \omega_z^2 z^2\right)$), such as we find in quantum dots. The proof of GKT is reasonably straightforward, and the essential aspects of the proof will be presented here.

Consider an gas of N electrons confined to the z=0 plane (i.e., a 2DEG) and constrained laterally by the harmonic potential $V = \frac{m^*\omega_0^2}{2}r^2$, where $r = (x^2 + y^2)^{\frac{1}{2}}$. If this system (already a quantum dot) is placed in a uniform magnetic field oriented along the z-axis, the Hamiltonian of the system is

$$H = \sum_{\alpha=1}^{N} \frac{1}{2m^*}\left(\pi_{x_\alpha}^2 + \pi_{y_\alpha}^2\right) + \frac{m^*}{2}\left(\omega_x^2 x_\alpha^2 + \omega_y^2 y_\alpha^2\right) + \sum_{\alpha,\beta} U\left(\mathbf{r}_\alpha - \mathbf{r}_\beta\right), \qquad \text{(B.10)}$$

where α is the electron index, π_α is the canonical momentum (i.e., $\pi_\alpha = \mathbf{p}_\alpha - \frac{e}{c}\mathbf{A}\left(\mathbf{r}_\alpha\right)$), and the last term represents the electron-electron interaction. The vector potential A allows for the inclusion of the perpendicular magnetic field and the EM field.

The proof of the theorem rest essentially with two algebraic manipulations. First, we apply the identity for quadratic forms to the Hamiltonian, then we rewrite the result in terms of centre of mass and relative coordinates and momenta. There are several ways to choose centre of mass and relative coordinates which ensure that we maintain a complete basis set for system's phase space. The choice used here is fairly common in the literature. We define the centre of mass variables

as

$$\mathbf{R}_{cm} = \frac{1}{N}\sum_{\alpha=1}^{N}\mathbf{r}_{\alpha}, \tag{B.11}$$

$$\mathbf{\Pi}_{cm} = \sum_{\alpha=1}^{N}\pi_{\alpha}, \tag{B.12}$$

and the relative variables as

$$\mathbf{r}_{rel_i} = \sum_{\alpha=1}^{i}\mathbf{r}_{\alpha} - (i-1)\,\mathbf{r}_i, \tag{B.13}$$

$$\text{and } \pi_{rel} = \sum_{\alpha=1}^{i}\pi_{\alpha} - (i-1)\,\pi_i. \tag{B.14}$$

for $i = 2, \cdots, N$. The identity for quadratic forms is

$$\sum_{\alpha}^{N} q_{\alpha}^2 = \frac{1}{N}\left(\sum_{\alpha}^{N} q_{\alpha}\right)^2 + \frac{1}{N}\sum_{\alpha,\beta:\alpha<\beta}^{N}(q_{\alpha}-q_{\beta})^2, \tag{B.15}$$

where q_{α} may represent any of the space or momentum coordinates. When we apply this to the Hamiltonian given above, we get

$$\begin{aligned} H = {} & \frac{1}{2Nm^*}\left(\sum_{\alpha=1}^{N}\pi_{\alpha}\right)^2 + \frac{1}{2Nm^*}\sum_{\alpha,\beta:\alpha<\beta}^{N}(\pi_{\alpha}-\pi_{\beta})^2 + \frac{m^*\omega_x^2}{2N}\left(\sum_{\alpha=1}^{N}x_{\alpha}\right)^2 + \frac{m^*\omega_x^2}{2N}\sum_{\alpha,\beta:\alpha<\beta}^{N}(x_{\alpha}-x_{\beta})^2 \\ & + \frac{m^*\omega_y^2}{2N}\left(\sum_{\alpha=1}^{N}y_{\alpha}\right)^2 + \frac{m^*\omega_y^2}{2N}\sum_{\alpha,\beta:\alpha<\beta}^{N}(y_{\alpha}-y_{\beta})^2 + \sum_{\alpha,\beta}U\left(\mathbf{r}_{\alpha}-\mathbf{r}_{\beta}\right), \end{aligned} \tag{B.16}$$

to which we can apply our definitions of the centre of mass and relative variables. Notice that the first, third and fifth terms can be expressed in terms of the centre of mass variables, while the second, fourth, sixth and seventh terms are all functions of the relative coordinates. Rewriting this Hamiltonian in terms of the centre of mass variables yields

$$H = \frac{1}{2Nm^*}\mathbf{\Pi}_{cm}^2 + \frac{Nm^*\omega_x^2}{2}X_{cm}^2 + \frac{Nm^*\omega_y^2}{2}Y_{cm}^2 + \frac{1}{2Nm^*}\sum_{\alpha,\beta:\alpha<\beta}^{N}(\pi_{\alpha}-\pi_{\beta})^2$$

$$+\frac{m^*\omega_x^2}{2N}\sum_{\alpha,\beta;\alpha<\beta}^{N}(x_\alpha-x_\beta)^2+\frac{m^*\omega_y^2}{2N}\sum_{\alpha,\beta;\alpha<\beta}^{N}(y_\alpha-y_\beta)^2+\sum_{\alpha,\beta}U(\mathbf{r}_\alpha-\mathbf{r}_\beta),$$

(B.17)

and we readily see that the Hamiltonian has been separated into centre of mass and relative motion variables. We write this as

$$H=H_{cm}+H_{rel},$$

where

$$H_{cm}=\frac{1}{2Nm^*}\mathbf{\Pi}_{cm}^2+\frac{Nm^*}{2}\left(\omega_x^2X_{cm}^2+\omega_y^2Y_{cm}^2\right), \tag{B.18}$$

and

$$H_{rel}=\frac{1}{2Nm^*}\sum_{\alpha,\beta;\alpha<\beta}^{N}(\pi_\alpha-\pi_\beta)^2+\frac{m^*\omega_x^2}{2N}\sum_{\alpha,\beta;\alpha<\beta}^{N}(x_\alpha-x_\beta)^2+\frac{m^*\omega_y^2}{2N}\sum_{\alpha,\beta;\alpha<\beta}^{N}(y_\alpha-y_\beta)^2+\sum_{\alpha,\beta}U(\mathbf{r}_\alpha-\mathbf{r}_\beta)$$

(B.19)

Notice that we can now write the centre of mass canonical momentum as

$$\mathbf{\Pi}_{cm}=\mathbf{P}_{cm}-\frac{Ne}{c}\mathbf{A}(\mathbf{R}_{cm}),$$

and that the new centre of mass Hamiltonian looks like the Hamiltonian for a single electron of mass Nm^* and charge Ne.

We can determine by direct calculation that the commutation relations for the centre of mass and momentum variables are

$$[\Pi_{cm},x_{rel}]=[\Pi_{cm},y_{rel}]=[X_{cm},\pi_{rel}]=[Y_{cm},\pi_{rel}]=0,$$

and with these in hand we can show that

$$[H_{cm},H_{rel}]=0.$$

Standard quantum mechanics then implies that the eigenstates of H can be written as the product state

$$|\Psi\rangle = |\Psi_{cm}\rangle\,|\Psi_{rel}\rangle\,,$$

and so we see that centre of mass motion and relative motion separate completely for our system.

Now consider the behavior of this system under a spatially homogenous, time varying electric field of the form

$$\mathbf{E}\,(t) = \mathbf{E}_0 e^{-i\omega t},$$

which yields an interaction term for the αth electron of

$$H^I_\alpha = -e\mathbf{E}_0 \cdot \mathbf{r}_\alpha e^{-i\omega t}.$$

The interaction term representing all the electrons will be

$$\begin{aligned} H^I &= \sum_\alpha H^I_\alpha \\ &= \sum_\alpha \left(-e\mathbf{E}_0 \cdot \mathbf{r}_\alpha e^{-i\omega t}\right) \\ &= \left(-e\mathbf{E}_0 e^{-i\omega t}\right) \cdot \sum_\alpha \mathbf{r}_\alpha\,. \end{aligned} \tag{B.20}$$

Recall, however that $\mathbf{R}_{cm} = \frac{1}{N}\sum_\alpha \mathbf{r}_\alpha$, and so the interaction term can be written as

$$H^I = (-Ne)\,\mathbf{E}_0 \cdot \mathbf{R}_{cm} e^{-i\omega t}, \tag{B.21}$$

from which we can see that the electric field will interact only with the centre of mass Hamiltonian, since $\mathbf{R}_{cm}$ and hence H^I commute with the relative motion

coordinates. As previously mentioned, the centre of mass Hamiltonian for N electrons is identical to the Hamiltonian for a single particle of mass Nm^* and charge Ne, and such a particle will experience resonance at the cyclotron frequency of a single electron, since the mass of the particle and the force exerted on it by the electric field scale linearly with N.

Bibliography

[1] Walter Kohn, *Phys. Rev.* **123**, 1242 (1961).

[2] P. Ullersma, *Physica* **32**, 27 (1966).

[3] G. W. Ford, J. T. Lewis, and R. F. O'Connell, *J. of Stat. Phys.* **53**, 439 (1988).

[4] G. W. Ford, J. T. Lewis, and R. F. O'Connell, *Phys. Rev. A* **37**, p. 4419 (1988).

[5] A. B. Fowler, F. F. Fang, W. E. Howard, and P. J. Stiles, *Phys. Rev. Lett.* **16**, p. 901 (1966).

[6] R. Dingle, A. C. Gossard, and W. Wiegmann, *Appl. Phys. Lett.* **33**, 665 (1975).

[7] L. Esaki, *Proceedings of the Nobel Jubilee Symposium*, Ed. M. Jonson and T. Claeson, p.102, December 4-7, 1991.

[8] M. Reed, editor, *Nanostructured Systems* (Academic, New York, 1992), Chap. 1, p. 1.

[9] P. M. Petroff, A. C. Gossard, and W. Wiegmann, *Appl. Phys. Lett.* **45**, p. 620 (1984).

[10] E. Kapon, S. Simhony, R. Bhat, D. M. Hwang, *Appl. Phys. Lett.* **55**, No. 26, p. 2715 (1989).

[11] A. Chavez–Pirson, H. Ando, H. Saito, and H. Kanbe, *Appl. Phys. Lett.* **64**, p. 1759 (1994).

[12] C. Weisbuch, M. Nishioka, A. Ishikawa, and Y. Arakawa, *Phys. Rev. Lett.* **69**, p. 3314 (1992).

[13] M. A. Reed, J. N. Randall, R. J. Aggarwal, R. J. Matyi, T. M. Moore, and A. E. Wetsel, *Phys. Rev. Lett.* **60**, p. 535 (1988).

[14] J. Oshinowo, M. Nishioka, S. Ishida, and Y. Arakawa, *Appl. Phys. Lett.* **65**(11), p. 1421 (1994).

[15] O. V. Salata, P. J. Dobson, P. J. Hull, and J. L. Hutchison, *Appl. Phys. Lett.* **65**(2), p. 189 (1994).

[16] G. Rempe, R. J. Thompson, and H. J. Kimble, *Fundamentals of Quantum Optics III*–F. Ehlotzky(Ed.) (Springer-Verlag, New York, 1993), p. 197.

[17] Y. Zhu, D. J. Gautier, S. E. Morin, Q. Wu, H. J. Carmichael, and T. W. Mossberg, *Phys. Rev. Lett.* **64**(21), p. 2499 (1990).

[18] L. Brey, N. F. Johnson, and B. I. Halperin, *Phys. Rev. B* **40**(15), p. 10647 (1989).

[19] John F. Dobson, *Phys. Rev. Lett.* **73**(16), p. 2244 (1994).

[20] S. K. Yip, *Phys. Rev. B* **43**(2), p. 1707 (1991).

[21] J. Ciebert, P. M. Petroff, G. L. Dolan, S. J. Pearton, A. C. Gossard, and J. H. English, *Appl. Phys. Lett.* **49** (19), p. 1275 (1986).

[22] Garnett W. Bryant, *Phys. Rev. Lett.* **59** (10), p. 1140 (1987).

[23] R. B. Laughlin, *Phys. Rev. B* **27** (6), p. 3383 (1983).

[24] Wei-Ming Que and George Kirczenow, *Phys. Rev. B* **38**, p. 3614 (1988).

[25] D. Pfannkuche and S. E. Ulloa, *Phys. Rev. Lett.* **74** (7), p. 1194 (1995).

[26] Ch. Sikorski and U. Merkt, *Phys. Rev. Lett.* **62** (18), p. 2164 (1989).

[27] C. T. Liu, K. Nakamura, D. C. Tsui, K. Ismail, D. A. Antoniadis, and H. I. Smith, *Appl. Phys. Lett.* **55**, p. 168 (1989).

[28] T. Demel, D Heitmann, P. Grambow, and K. Ploog, *Phys. Rev. Lett.* **64** (7), p. 788 (1990).

[29] V. Fock, *Z. Phys.* **47**, p. 446 (1928).

[30] P. A. Maksysm and Tapash Chakraborty, *Phys. Rev. Lett.* **65** (1), p. 108 (1990).

[31] P. Bakshi, D. A. Broido, and K. Kempa, *Phys. Rev. B* **42** (12), p. 7416 (1990).

[32] D. A. Broido, K. Kempa, and P. Bakshi, *Phys. Rev. B* **42** (17), p. 11400 (1990).

[33] J. R. Schrieffer, *Mobility in Inversion Layers: Theory and Experiment*, in *Semicondoctor Surface Physics Ed. R. H. Kingston (Univ. of Pennsylvania Press)*, p. 55 (1957).

[34] Frank Stern and W. E. Howard, *Phys. Rev.* **163** (3), p. 816 (1967).

[35] T. Ando, *Phys. Rev. B* **13**, p. 3468 (1976).

[36] P. Hohenberg and W. Kohn, *Phys. Rev.* **136**, p. B864 (1964).

[37] W. Kohn and L. J. Sham, *Phys. Rev.* **140**, p. A1133 (1965).

IMAGE EVALUATION
TEST TARGET (QA-3)

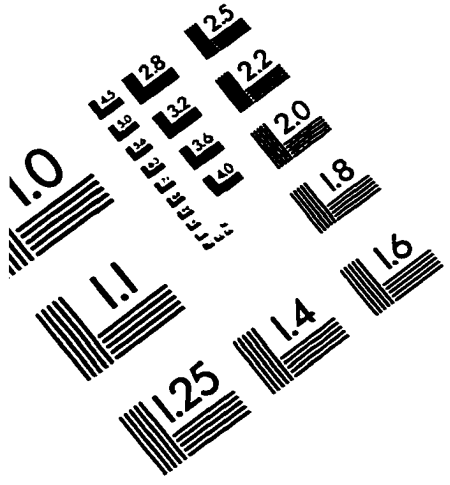

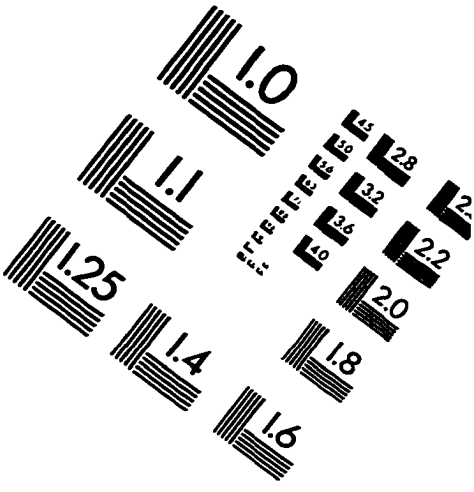

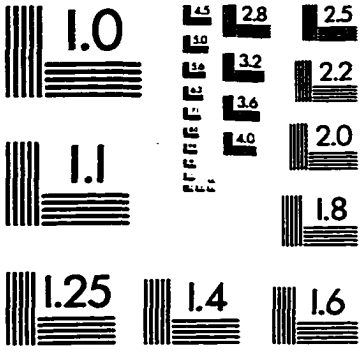

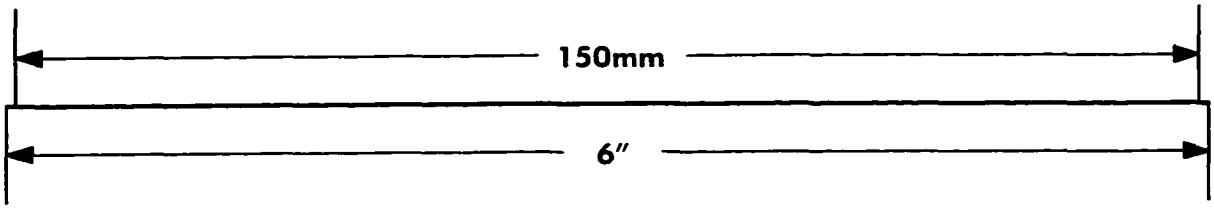

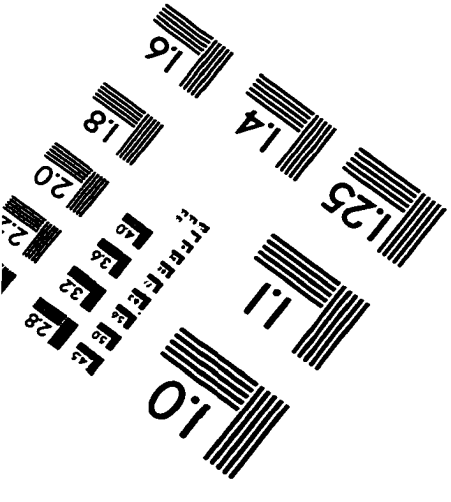

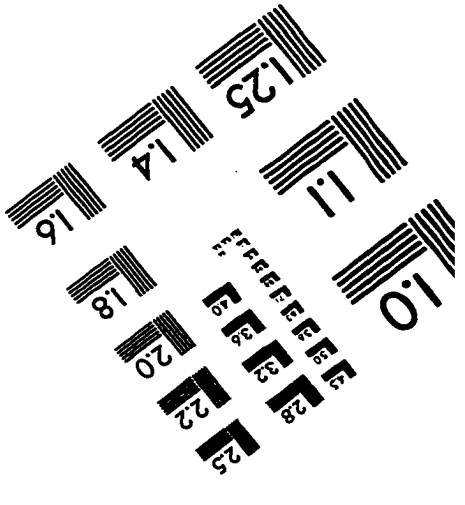

APPLIED IMAGE, Inc
1653 East Main Street
Rochester, NY 14609 USA
Phone: 716/482-0300
Fax: 716/288-5989